Membrane Association, Electrostatic Sequestration, and Cytotoxicity of Gly-Leu-Rich Peptide Orthologs with Differing Functions†

Damien Vanhoye, Francine Bruston, Shaharazade El Amri, Ali Ladram, Mohamed Amiche, and Pierre Nicolas*

Laboratoire de Bioactivation des Peptides, Institut Jacques Monod, 2 Place Jussieu, 75251 Paris Cedex 05, France

Received April 7, 2004; Revised Manuscript Received May 4, 2004

ABSTRACT: The skins of closely related frog species produce Gly-Leu-rich peptide orthologs that have very similar sequences, hydrophobicities, and amphipathicities but differ markedly in their net charge and membrane-damaging properties. Cationic Gly-Leu-rich peptides are hemolytic and very potent against microorganisms. Peptides with no net charge have only hemolytic activity. We have used ancestral protein reconstruction and peptide analogue design to examine the roles of electrostatic and hydrophobic interactions in the biological activity and mode of action of functionally divergent Gly-Leu-rich peptides. The structure and interaction of the peptides with anionic and zwitterionic model membranes were investigated by circular dichroism with 2-dimyristoyl-*sn*-glycero-3-phosphatidylcholine or 1,2-dimyristoyl-*sn*-glycero-3-phosphatidylglycerol vesicles and surface plasmon resonance with immobilized bilayers. The results, combined with antimicrobial assays, the kinetics of bacterial killing, and membrane permeabilization assays, reveal that Gly, Val, Thr, and Ile can all be accommodated in an amphipathic α helix when the helix is in a membrane environment. Binding to anionic and zwitterionic membranes fitted to a 2-stage interaction model (adsorption to the membrane followed by membrane insertion). The first step is governed by hydrophobic interactions between the nonpolar surface of the peptide helix and the membranes. The strong binding of Gly-Leu-rich cationic peptides to anionic membranes is due to the second binding step and involves short-range Coulombic interactions that prolong the residence time of the membrane-inserted peptide. The data demonstrate that evolution has positively selected charge-altering nucleotide substitutions to generate an orthologous cationic variant of neutral hemolytic peptides that bind to and permeate bacterial cell membranes.

The interactions of peptides with cellular membranes are of fundamental importance in the functioning of numerous membrane-mediated processes including signal transduction, intracellular signaling, hormone receptor interactions in which the accumulation of ligands on the membrane surface precedes the binding of the ligand to its receptor, channel formation, viral fusion processes, and antimicrobial and cytolytic peptide action. Investigations of the binding properties of membrane-interacting peptides and membrane-damaging peptides are also designed to show how the molecular environment versus the primary structure of a protein affects its folding and stability. They could thus have a marked impact on our ability to combat cytotoxic diseases such as type II diabetes (*1*, *2*), Creutzfeldt−Jacob (*3*), and Alzheimer diseases (*4*), as well as the growing problem of pathogenic microorganisms that are resistant to conventional antibiotics (*5*−*7*).

Membrane-damaging peptides that play a role in the defense against competing or attacking organisms are small proteins, typically 10−50 residues long, that interact with lipid bilayers to alter cell-membrane permeability, which often leads to cell death (*8*). Most of these peptides have little, if any, target specificity and may act on many membrane types including those of bacteria, protozoan, yeasts, fungi, and mammalian cells (*9*−*19*). Structural studies have revealed that peptide secondary structures include α helixes, β-sheet structures stabilized by 2−3 disulfide bonds, extended structures with an overrepresentation of one or two amino acids (W, P, H), and cyclic peptides (*20*−*23*). However, all of these peptides, regardless of the secondary structure or length, exhibit amphipathic properties upon interaction with lipid bilayers, with apolar amino acid residues segregating from the hydrophilic residues on opposite sides of the three-dimensional structure. It is generally assumed that this common feature enables the peptides to interact optimally with the amphipathic structure of the membrane, leading to permeation and disruption of the target cell. Three general and nonexclusive mechanisms, the barrel-stave model (*24*), micellar aggregates, and carpet model (*25*−*29*) have been proposed to describe the process of membrane permeation/disruption by defense peptides. The main difference between these models is that the barrel-stave one requires a few peptide molecules to assemble and form a transmembrane pore in the membrane, whereas the two other models require the surface of the membrane to be coated with the peptide to a critical concentration before it cracks, disrupts, and causes the cytoplasmic components to leak out.

Only few antimicrobial peptides of eukaryotic origin that are not toxic or moderately so to most normal mammalian

† Supported by funds from the CNRS.

* To whom correspondence should be addressed: Laboratoire de Bioactivation des Peptides, Institut Jacques Monod, UMR 7592 CNRS/Université Paris 6 et Université Paris 7, 2 Place Jussieu, 75251 Paris Cedex 05, France. Phone: 01 44 27 69 52. Fax: 01 44 27 59 94. E-mail: pnicolas@ccr.jussieu.fr.

10.1021/bi0493158 CCC: $27.50
Published on Web 06/09/2004

cells retain a high microbicidal activity. They have been isolated from a variety of sources including the frog skin where they function primarily by providing an effective and fast-acting defense against harmful microorganisms (*30*−*35*). Most of these peptides are amphiphatic α-helical peptides that are positively charged because of their Lys and/or Arg content. It has thus been proposed that the high content of anionic lipids in prokaryotic membranes and their absence from the neutral matrix of erythrocytes account for the preferential binding of cationic peptides to the outer leaflet of bacterial bilayers through nonspecific long-range electrostatic interactions. Although this can provide microbial specificity, several studies have convincingly demonstrated that antibacterial versus hemolytic activity is mediated by a complex, sensitive balance between various peptide parameters including the charge, hydrophobicity, degree of structure formation, amphipathicity, size of the polar/apolar sectors, and flexibility (*36*−*49*). However, the exact role of each parameter may change from one peptide to another. These studies also showed that there is no simple correlation between peptide charge, antimicrobial activity, and toxicity for eukaryotic cells. For instance, several cytotoxic peptides that are positively charged are unselective with respect to the anionic bacterial membrane by a simple electrostatic interaction between basic residues of the peptide and negatively charged groups of the membrane outer leaflet. There are also anionic peptides that are antimicrobial (*50*). Another important question that remains to be answered is whether charge-induced activity and selectivity for bacterial cells are due only to changes in lipid affinity or whether differences in the membrane-disturbing activity of the bound peptide are also involved. These difficulties might arise from the strategies that have been used (comparative analysis of sequences of naturally occurring antimicrobial peptides and hemolytic peptides, use of combinatorial libraries, and studies of the structural properties of peptides and analogues in membrane interactions), most of them relying on comparing peptides that differ in more than one parameter. Further understanding of the role of electrostatic and hydrophobic interactions in the binding of α-helical peptides to anionic membrane and their permeation/disruption would be aided by analysis of peptides that are very closely related but differ markedly in their cell selectivity.

The sequence of proteins from ancient organisms can be reconstructed from the sequences of their descendants, prepared in the laboratory, and studied (*51*). This report describes the evolution of a novel antimicrobial function during speciation in which Darwinian (positive) selection operated at a molecular level. We cloned and isolated Gly-Leu-rich, membrane-disruptive peptide orthologs whose precursor polypeptides belong to the dermaseptin family, from the skin of closely related species of South American hylid frogs of the Phyllomedusinae subfamily. The precursors of this family have a common N-terminal preproregion that is remarkably well-conserved both within and between species but have a hypervariable C-terminal domain corresponding to antimicrobial peptides with very different lengths, sequences, charges, and antimicrobial spectra (*52*). These include the dermaseptins B and dermaseptins S, phylloxin, and dermatoxin, from frogs of the *Phyllomedusa* genus (*52*−*54*), several dermaseptin-related peptides, designated DRP-AA[1] (from *Agalychnis annae*) and DRP-PD (from *Pachymedusa dacnicolor*) (*55*), and the caerins (*31*) that are produced by Australian frogs of the genus *Litoria* (family = Hylidae, subfamily = Pelodryadinae). The diversity of these peptides is due to multiple duplications of a common ancestral gene before and during radiation of the species and within individual species (*52*). The Gly-Leu-rich peptide orthologs all have very similar amino acid sequences, hydrophobicities, and amphipathicities but differ markedly in their activity spectra. Whereas positively charged and neutral peptides are hemolytic peptides, only cationic peptides have potent antimicrobial activity against a broad spectrum of microorganisms. Reconstruction of the ancestral protein and the design of peptide analogues suggest that positive selection operated in the early stages of frog species divergence to produce a novel antimicrobial function from an otherwise inactive ancestral peptide and that lysine residues were selected. We also find that α-helical folding of cationic Gly-Leu-rich peptides at anionic and zwitterionic membrane interfaces is driven by the hydrophobic effect. In sharp contrast to most other known cationic antimicrobial peptides, selection of anionic versus zwitterionic membranes by Gly-Leu-rich peptides arises from short-range electrostatic interactions that elongate the residence time of the peptide inserted in the membrane.

MATERIALS AND METHODS

Frog Species. Specimens of *Agalychnis callydryas* and *P. dacnicolor* were obtained from "La Ferme Tropicale" (Paris, France). Specimens of *Phyllomedusa bicolor* were housed in large wooden cages (120 × 90 × 90 cm), covered on three sides by plastic mosquito net (*56*). Phyllodendron, Potos, and Dracena were used as perches, and water bowls were provided for nocturnal baths. The frogs were fed crickets. The relative humidity was maintained at 65% with a humidifier. The temperature was kept at 25 ± 1 °C.

cDNA Cloning. Specimens of *Agalychnis callydryas* and *P. bicolor* were anesthetized with pentobarbital; the skin was removed and placed on dry ice. A sample (180 mg) of skin was homogenized with polytron and the poly(A+) RNAs were isolated by running the homogenate through an affinity oligo (dT) spin cellulose column (Invitrogen, Micro-Fast-Track kit). The cDNA was synthesized by RT-PCR, with 3′ RACE (Invitrogen) using a 5′ primer (5′-GGCTTCCCTG-AAGAAATCTC-3′) corresponding to the nucleotide sequence encoding the conserved N terminus of the preproregion of dermaseptin precursors (*56*) and a primer specific to the 3′ adaptator under the following conditions: 35 cycles of 94 °C for 240 s, 56 °C for 45 s, 72 °C for 60 s, and one cycle of 72 °C for 10 min. The PCR product was cloned in the pGEMt-easy vector system (Promega) using standard procedures (*57*) and used to transform competent JM 109

[1] Abbreviations: CD, circular dichroism; DMPC, 1,2-dimyristoyl-*sn*-glycero-3-phospha-tidylcholine; DMPG, 1,2-dimyristoyl-*sn*-glycero-3-phosphatidylglycerol; DRP, dermaseptin-related peptide; HPLC, high-performance liquid chromatography; LUVs, large unilamellar vesicles; MALDI−TOF, matrix-assisted-laser-desorption/ionization time-of-flight; ONPG, *o*-nitrophenyl β-D-galactopyranoside; PBS, phosphate-buffered saline; PCR, polymerase chain reaction; RACE, rapid amplification of cDNA ends; RU, resonance unit; SPR, surface plasmon resonance; TFA, trifluoracetic acid.

Escherichia coli. The white positive colonies of transformed *E. coli* were screened with T7 (5′-ATTATGCTGAGTGATACCCGCT-3′) and SP6 (5-ATTTAGGTGACACTATAGAATAC-3′) primers. Amplification products of the expected sizes (400−500 bp) were sequenced by the dideoxy chain terminator method. We determined the sequences of the 5′ end of the prepro-DRP-PBN2, prepro-DRP-AC1, and DRP-AC2 with the cDNA as a template in RACE PCR with sense primers specific to the 5′ adaptator and a specific antisense primer (Figure 3). The temperature cycle used for the RACE PCRs was 94 °C for 240 s, 35 cycles at 94 °C for 40 s, 56 °C for 45 s, 72 °C for 60 s, and a final extension step of 72 °C for 10 min. The PCR products were cloned and sequenced as above.

Tissue Distribution. Samples of mRNA from frog skin, brain, and intestine were prepared using the Micro-FastTrack kit (Invitrogen) and amplified by RT-PCR using the SuperScript One-Step RT-PCR System (Life Technologies). Both cDNA synthesis and PCR were performed in a single tube using specific primers deduced from the skin prepro-DRP-PBN2 (sense primer 1 = 5′-ATTACAA GATCAGTCATGGC-3′, and antisense primer 2 = 5′-TCTTAACTTTGACCACCTGTCACTG-3′) and mRNA from frog brain, skin, or intestine. The thermal cycle profile used for the RT-PCR was 45 °C for 30 min and then 94 °C for 2 min, followed by 30 cycles of 94 °C for 40 s, 55 °C for 30 s, 72 °C for 60 s, and a final extension step of 72 °C for 5 min. This was followed by nested PCR using sense primer 3 = 5′-ATGGCTT TCCTGAAGAAATC-3′ and an antisense primer 4 = 5′-TGTCACTGAACCAAACAGACC-3′. The thermal cycle profile was 94 °C for 240 s and then 72 °C for 1 min, followed by 30 cycles of 94 °C for 40 s, 55 °C for 30 s, and 72 °C for 5 min. PCR products were purified using a Qiaquick Kit, cloned in pGEMT-Easy vector (Promega), and sequenced as above.

Sequence Analysis. The nucleotide sequences of cDNAs encoding DRP-PBN2, DRP-AC1, and DRP-AC2, together with that of 27 known dermaseptins B, phylloxins, dermatoxins, dermaseptin-related peptides, and caerins from the hylids *P. bicolor*, *A. annae*, *P. dacnicolor*, and *Litoria caerulea* were aligned with Clustal X (*58*) and by eye. We first aligned the predicted amino acid sequences of the different domains of the preproforms and nucleotide sequences of the 5′- and 3′-untranslated regions with Clustal X. We then added the nucleotide sequences of the different regions and finally adjusted the alignment manually. Molecular phylograms from the alignments were determined with neighbor joining from Kimura two-parameter distances (*59*) using PAUP (*60*). Support for branches was estimated by bootstrapping (1000 replicates), also with PAUP. Sequence groups were denoted based on the existence of distinct clades and similarity of predicted amino acid sequences. We estimated the proportion of synonymous substitutions per synonymous sites (Ds) and the proportion of nonsynonymous substitutions per nonsynonymous sites (Dn) from the beginning of the preproregion to the last codon before the stop codon by method I of Ina (*61*) to determine if different gene regions mutate at different rates. For comparison, Jukes−Cantor distances (*62*) were estimated for the 5′- and 3′-untranslated regions using the same program.

Purification of DRP-PBN2 and DRP-PD 3−6 from Frog Skin Extracts. The skins of 2 specimens, one of *P. bicolor* and one of *P. dacnicolor* (1 g/skin) were minced with scissors and extracted using a Polytron in 20 volumes (v/w) of 80% methanol/water at 4 °C. The extracts were centrifuged for 30 min at 3000*g*, and the supernatants were lyophilized. The dried extracts were dissolved in 0.1% TFA/water and applied to a Waters RCM compact preparative cartridge (Deltapak C 18, 100 × 25 mm) and eluted at 0.75 mL/min with a 20−80% linear gradient of acetonitrile containing 0.07% TFA. Fractions (1 mL) were collected. The molecular masses of the peptides in each fraction were determined by MALDI−TOF mass spectrometry (*63*). Peptides of $m/z = 2000-4000$ were then purified on the same HPLC column developed with the same solvent system.

Sequencing by Nanoelectrospray Tandem Mass Spectrometry. The nanoelectrospray experiments were done on a triple quadrupole Bio-Q mass spectrometer, upgraded by the manufacturer so that the source and the quadrupoles had Quattro II performance (Micromass Ltd., U.K., Altrincham). The conventional electrospray probe was modified so that a glass capillary similar to that described by Wilm and Mann (*64*) could be placed about 2 mm from the first cone of the electrospray source. The source was used without a counter electrode, and the drying gas at 50 °C was nitrogen. The glass capillary voltage was 900 V, and that of the extracting cone was 50 V. Electrical contact between the tip of the probe and the metallized glass capillary (long-needle-type glass capillaries purchased from the Protein Analysis Compagny, Odense M) was made by placing a graphite cone inside the Swagelok union instead of the customary brushing with an organic solution of graphite (*64*) that gives interference ions in the low *m*/*z* range. The glass capillary was opened by briefly touching it with a metal capillary (0.5-mm inner diameter × 150 mm), connected to a vacuum source, and washed with N_2 under pressure to reduce contamination by impurities in the metal layer. The sample solution (1 pmol/μL in acetonitrile/water) was placed in the glass capillary, and the capillary was inserted into the MS source. Static air pressure was applied to give a flow rate of approximately 20 nL/min, which provided a stable signal for up to 3 h. The parent ion (m/z = 1064.0382 for DRP-PD36 and 806.7760 for DRP-PBN2) produced at a low cone voltage (Vc = 30 V) was first selected in the first quadrupole mass analyzer and fragmented by collision-induced dissociation with argon gas at 4.5×10^{-2} Pa at 40 V. Additional structural information was obtained by carrying out MS−MS experiments on fragments generated by source collision of the parent ion at *m*/*z* definite with an extracting cone voltage of 100 V using 60 and 80 V in the collision cell. The resulting fragment ions were named according to the nomenclature Roepstoff and Fohlman (*65*). The quadrupole analyzers were calibrated using the multiply charged ions from an acquisition of angiotensine.

Solid-Phase Peptide Synthesis. DRP-PBN2, DRP-PBN2 amide, DRP-PD 3−6, ANC, [K^8, K^{12}]-ANC, [K^8, K^{12}]-DRP-PD 3−6, [K^8, K^{12}, F^{18}]-DRP-PD 3−6, and DRP-PBN1 were synthesized using solid-phase FastMoc chemistry on an Applied Biosystems 433A Automated Peptide Synthesizer (Applera, France). Fmoc-protected amino acids and resins were from Senn Chemicals (Switzerland), and solvents were

from sds (France). The carboxylic acid terminal peptides were prepared on a 4-benzyloxybenzyl alcohol resin (Wang PS resin) substituted at 1.18 mmol/g. Carboxamidated peptides were prepared on a 4-methylbenzhydrylamine polystyrene resin (Rink Amide MBHA PS resin) substituted at 0.81 mmol/g. Synthesis was carried out using a double-coupling protocol: Fmoc amino acids (10 molar excess) were coupled for 30−60 min with 2-(1H-benzotriazol) in dimethylformamide with diisopropylethylamine and *N*-methylpyrrolidone as activating agents. Capping with acetic anhydride was performed at the end of each cycle. Temporary N-Fmoc protecting groups were removed with 20% piperidine in *N*-methyl-2-pyrrolidone. Side chains were protected with *tert*-butyloxycarbonyl (*t*Boc) for lysine; *O-tert*-butyl ester (*Ot*Bu) for aspartic acid; trityl (Trt) for threonine, glutamine, and asparagine; *O-tert*-butyl ether (*t*Bu) for serine. The peptidyl resin was cleaved, and the side chain was deprotected by incubation in 95% trifluoroacetic acid, 2.5% triisopropylsilane, and 2.5% water for 2 h at room temperature. The resulting mixture was filtered to remove the resin, and the crude peptides were precipitated with ether at −20 °C. They were recovered by centrifugation at 5000*g* for 15 min at 4 °C, washed 3 times with cold ether, dried under a stream of nitrogen, dissolved in 10% acetic acid, and lyophilized. The lyophilized crude peptides were purified by reverse-phase HPLC on a Nucleosil C18 column (5 μm, 10 × 250 mm) eluted at 4 mL/min with a 0−60% linear gradient of acetonitrile in 0.07% trifluoroacetic acid/water over 30 min. The homogeneity of the synthetic peptides was assessed by MALDI−TOF mass spectrometry (Voyager DE RP, Perseptive Biosystems) and analytical HPLC (*63*).

Energy Minimization and Electrostatic Potential Distributions. Peptides were constructed as ideal α helices, and then 1000 energy minimization steps were performed using DISCOVER 3 (Insight II, Accelrys, Inc.) with a CVFF force field. Electrostatic free energies were derived from finite difference solutions of the Poisson−Boltzmann equation using Delphi (Insight II, Accelrys, Inc.) (66, 67). Full Coulombic calculations were performed using a boundary extending 10 Å beyond the longest axis of the peptide. The internal peptide dielectric constant was 5, and the solvent dielectric constant was 80. An energy convergence criterion of 1×10^{-6} kcal/mol was applied. Calculations were carried out on an O_2 R10000 Silicon Graphics workstation.

Antimicrobial Assays. Gram-positive eubacteria (*Bacillus megaterium, Bukholderia cepacia, Staphylococcus aureus, Staphylococcus haemolyticus*, and *Streptococcus pneumoniae*), Gram-negative eubacteria (*E. coli B, Enterobacter cloacae, Clostridium perfringens, Klebsiella pneumoniae, Listeria monocytogenes, Neisseria meningitides, Pseudomonas aeruginosa, Salmonella typhimurium, Salmonella enteritidis*, and *Vibrio cholera*), and yeasts (*Candida albicans* and *Saccaromyces cerevisiae*) were cultured (*68*), and the minimal inhibitory concentrations (MICs) of peptides were determined. The bacteria were grown in 96-well microtitration plates in the presence of 2-fold serial dilutions of the peptide. Aliquots (10 μL) of each serial dilution were incubated with 100 μL of a suspension of a midlogarithmic phase culture of bacteria at a starting optical density of A_{630} = 0.001 in Poor-Broth nutrient medium [1% bactotryptone and 0.5% NaCl (w/v)] or Yeast Peptone Glucose for *S. cerevisiae*. The inhibition of growth was assessed by measuring the optical density at A_{630} after 16 h at 37 °C (bacteria) or at 30 °C (yeast). The MIC was defined as the lowest concentration of peptide that inhibited the growth of ≥99% of the cells. Bacteria were incubated for 2 h with different concentrations of peptides and plated out on solid culture medium containing 1% noble agar to distinguish between bacteriostatic and bactericidal effects. The plates were subsequently incubated and examined daily for the formation of colonies. All assays were performed three times plus positive controls without the peptide and negative controls with 0.7% formaldehyde.

Hemolysis of Rat Red Blood Cells. The hemolytic activity of the peptides was determined using fresh rat erythrocytes. The blood was centrifuged, and the erythrocytes were rinsed three times with PBS (35 mM phosphate buffer and 0.15 M NaCl at pH 7.4). Peptides were incubated with the erythrocyte suspension (4% erythrocytes (v/v) in PBS) at 37 °C for 60 min, and the erythrocytes were removed by centrifugation at 800*g* for 10 min. Hemolysis was assessed by measuring the optical density at 540 nm of the supernatant. Erythrocytes lysed with 1% Triton X-100 were used as a standard for 100% hemolysis.

Kinetics of Bactericidal Activity. Bacteria were incubated overnight in Luria−Bertani medium and diluted with the medium to 0.1 OD. They were then incubated with the desired concentrations of peptides. Samples (100 μL) were removed at 0, 5, 10, 15, 30, 45, 60, 120, and 180 min and diluted 10^{1-8}-fold with PBS. Aliquots (1 mL) of these mixtures were placed on LB/agar plates and incubated overnight at 37 °C. Colonies were counted. Bactericidal activity was recorded as the number of surviving colonies after incubation with the peptides.

Peptide-Induced Permeabilization of the Cytoplasmic Membrane of E. coli. The permeabilization of the cytoplasmic membrane of *E. coli* K514 by Gly-Leu-rich peptides was assayed by measuring the β-galactosidase activity with the chromogenic substrate ONPG. *E. coli* K514 (wild type) was grown in 10% Luria−Bertani broth in the presence of 100 μg/mL IPTG (Sigma) to induce the enzyme. Bacteria were washed twice with 10% LB in PBS (0.15 M phosphate and 0.2 M NaCl at pH 7.4) and diluted to an OD_{630} of 0.5 in 10% LB in PBS. Aliquots (50 μL) of bacterial suspension were then mixed with 2 mM ONPG and incubated with various concentrations of peptides. The hydrolysis of ONPG was monitored by measuring the absorbance at 400 nm of released *o*-nitrophenol. Complete permeabilization was assessed using sonicated bacteria. All of the results are the means of 3−5 independent experiments.

Preparation of Large Unilamellar Vesicles (LUV). 2-Dimyristoyl-*sn*-glycero-3-phospha-tidylcholine (DMPC) and 1,2-dimyristoyl-*sn*-glycero-3-phosphatidylglycerol (DMPG) were purchased from Avanti Polar Lipids. Phospholipid vesicles were prepared by extrusion, and their average diameter (100 ± 20 nm) was estimated by turbidimetry at 436 nm using a 1-cm path length cuvette as described (*69*). Briefly, dry DMPC (30 mg) was dissolved in chloroform, or in the case of DMPG, the dry lipid was dissolved in a 2:1 (v/v) chloroform/methanol mixture. The solvents were evaporated off under a stream of nitrogen, and the lipids were held under a vacuum for 20 min. The dried lipids were

hydrated by vortexing and/or sonicating in 50 mM phosphate buffer (pH 7) plus 150 mM NaCl. The resultant lipid dispersion (14 mM with respect to phospholipids) was extruded 10 times through decreasing pore size filters (from 800 to 100 nm) to obtain 100 nm LUV. They were stored at 4 °C.

Circular Dichroism (CD) Spectroscopy. The CD spectra of the peptides were recorded with a Jasco J-810 Circular Dichroism spectropolarimeter (Jasco Corp., Tokyo, Japan) linked to a PC microprocessor. The instrument outputs were calibrated with D(+)-10-camphorsulfonic acid. The spectra were scanned at 25 °C in a quartz-optical cell with a 1-mm path length. Spectral measurements were obtained at wavelengths of 190−250 nm, at a scan rate of 20 nm/min with a bandwidth of 1 nm. Typically five scans were accumulated and averaged. The CD spectrum of each peptide was measured in 0.05 M phosphate buffer (pH 7) and, in the presence of increasing concentrations (30−1800 μM) of DMPC or DMPG vesicles, at a peptide concentration of 30 μM. The CD spectrum of the buffer and/or liposome solution without peptides was used as a baseline. CD measurements are reported as $\Delta\epsilon$ (M^{-1} cm^{-1}). The relative helix content was deduced according to Zhong and Johnson (*70*) as percent helix $= -[\Delta\epsilon_{222\ nm} \times 10]/n$, where $\Delta\epsilon_{222\ nm}$ is the dichroic increment at 222 nm and n is the number of residues in the peptide.

Binding Analysis by Surface Plasmon Resonance (SPR) Biosensor. Biosensor experiments were carried out at 25 °C with a Biacore 2000 biosensor (Biacore, Uppsala, Sweden) using L1 sensor chips (BIAcore). PBS (50 mM phosphate buffer at pH 7 plus 150 mM NaCl) was the running buffer. All solutions were degassed and filtered through a 0.22-μm filter. The L1 sensor chip contains hydrophobic aliphatic chains covalently linked to a dextran-coated gold surface. DMPC or DMPG LUVs (60 μL of 0.5 mM in 50 mM phosphate buffer at pH 7 plus 150 mM NaCl) were run onto the sensor chip (2 μL/min). The liposomes were captured on the surface of the sensor chip by the lipophilic compounds to produce a supported lipid bilayer. Multilamellar structures were removed by injecting a brief pulse (12 s) of 100 mM NaOH. This resulted in a stable signal of ~4000 resonance units (RU) for DMPG and 8000 RU for DMPC. Peptide solutions (60 μL of 1−30 μM peptide in PB for 180 s) were injected onto the bilayer surface at 20 μL/min to avoid limitation by mass transport. The peptide solution was then replaced by PBS, and the peptide−bilayer complex was allowed to dissociate for 180 s. The biosensor chip surface was regenerated by removing the bound phospholipids with an injection of 40 mM *n*-octyl D-glucopyranoside (100 μL at 10 μL/min). The SPR response (a change in resonance signal), expressed as RU, depends on the density of the peptide adsorbed onto the membrane. The affinity of the peptide for lipids was estimated from a series of response curves. The resulting sensorgrams were collected for several concentrations of each peptide interacting with each lipid surface. The peptide−lipid interaction sensorgrams were analyzed by curve fitting using numerical integration analysis (see beyond). Data were fitted globally by simultaneously fitting the peptide sensorgrams obtained in duplicate at 5 concentrations from 1 to 30 μM.

Three methods are currently used to calculate kinetic rate constants from biosensor data: linearization, curve fitting with analytical integration, and curve-fitting with numerical integration. Linearization can be used to estimate the rate constants when the analyte A binds to immobilized ligand B in a simple bimolecular or Langmuir interaction. However, our experimental sensorgramms do not fit the simple bimolecular model (see the Results). This may be the result of steric hindrance or a more complex interaction. Because a poor fit was obtained with the simple 1:1 binding model, the 2-state reaction model was used to determine the association and dissociation rate constants

$$P + L \leftrightarrow PL \leftrightarrow PL^*$$

where the peptide (P) binds to the lipid (L) to give the complex PL (primary binding). PL subsequently changes to PL*, which represents the penetration of the peptide into the hydrophobic core of the bilayer (*71*). PL* cannot dissociate directly to P and L. The rate constants and equilibrium affinity constants of each steps were determined by BIA biospecific interaction analysis using the BIA evaluation and BIA simulation software.

RESULTS AND DISCUSSION

Cloning of Gly-Leu-Rich Peptide Orthologs Encoded by the Hypervariable Domain of Dermaseptin Genes. 3′ RACE analysis of mRNAs from *P. bicolor* and *Agalychnis callidryas* (Family = Hylidae and subfamily = Phyllomedusinae) skin using a primer based on the conserved coding region of known preprodermaseptins revealed 3 novel cDNAs encoding 71−74 amino acid sequences starting with a Met codon and ending with a stop codon (Figure 1). The deduced amino acid sequences were all a 22-residue putative signal peptide followed by an acidic intervening sequence of 22−23 residues with a pair of basic residues Lys-Arg at its C terminus. A single copy of a mature peptide progenitor sequence was found at the extreme C terminus of the precursors flanked to the acidic propiece. The 3 prepropeptides all have the characteristic signature of the preproforms of the preprodermaseptin family, including a conserved signal peptide and acidic propiece whose amino acid sequences are 95 and 96% identical to those of other family members from South American and Australian hylid frogs (Figure 1). This similarity also extents into the 5′ and 3′ UTRs of the corresponding mRNAs (not shown). A comparison of the sequences of the 3 new cDNAs with those of preprodermaseptins from South American and Australian hylids indicates that they encode new putative peptides (DRP-PBN2, DRP-AC1, and DRP-AC2) that appear to be structurally related to DRP-AA 2−5 and DRP-PD 3−6, predicted from cDNA cloning of preprodermaseptins from *A. annae* and *P. dacnicolor* (*55*).

Because the true test of orthology is phylogeny, we analyzed the relationships among preprodermaseptin cDNAs from hylids, including the 3 new sequences, by neighbor joining and maximum parsimony. The hylid preprodermaseptins all seem to have arisen from a common ancestral gene, which subsequently diversified by several rounds of duplication and divergence of the duplicated copies (Figure 2). Most of the duplication predated the divergence of

A

```
                                                1/1                                                 31/11
          cgtccgcagcactgaattacaagatcagtc ATG GCT TTC CTG AAG AAA TCT CTC TTC CTT GTA
                                         M   A   F   L   K   K   S   L   F   L   V

                                    61/21                                           91/31
CTA TTC CTT GCA TTA GTT CCC CTT TCC ATC TGT GAA GAA AAG AAA AGT GAA GAG GAA AAT GAG
L   F   L   A   L   V   P   L   S   I   C   E   E   K   K   S   E   E   E   N   E

                                121/41                                      151/51
GAG AAA CAA GAA GAC GAT CAA AGC GAA GAG AAG AGA GGG CTG GTG ACA AGT CTA ATA AAA GGT
E   K   Q   E   D   D   Q   S   E   E   K   R   G   L   V   T   S   L   I   K   G

                              181/61
GCA GGG AAA TTG TTA GGA GGT CTG TTT GGT TCA GTG ACA GGT GGT CAA AGT taagaatatttaaaa
A   G   K   L   L   G   G   L   F   G   S   V   T   G   G   Q   S   *

tctaataaatctaattatcaatcattgtgtaaaaataaaatccagcatatttaactggtaaaaaaaaaaaaaaaaaaaaa
```

B

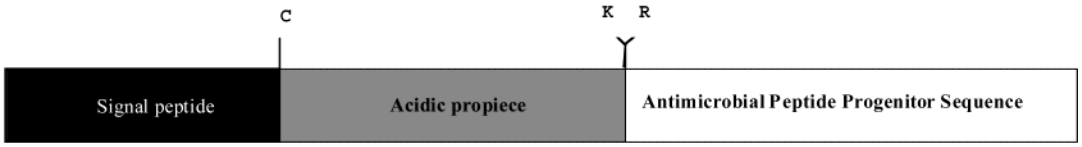


```
DRP-PBN2        MAFLKKSLFLVLFLALVPLSICEE-KKSEEENEEK-QEDD-Q---SEEKRGLVTSLIKGAGKLLGGLFGSVTGGQS
DRP-PD 3-6      MAFLKKSLFLVLFLALVPLSICEAEKREEENEEK--QEDDDE---SEKKRGVVTDLLNTAGGLLGNLVGSLSGGER
DRP-AC1         MAFLKKSLLLVLFLGLVSLSICEEEKRENEDEEK--QEDDDQ---SENKRGLLSGILNTAGGLLGNLIGSLSNGES
DRP-AC2         MAFLKKSLLLVLFLALVPLSICEEEKREEEDEEK--QEDDDQ---SENKRGLLSGILNSAGGLLGNLIGSLSNGES
DRP-AA 2-5      MAFLKKSLFLVLFLAIVPLSICEEEKREEENEEK--QEDDDQ---S--KRGLVSGLLNTAGGLLGDLLGSLGSLSGGES

DRS B1          MDILKKSLFLVLFLGLVSLSICEEEKRENEDEEK--Q-DDEQ---SEMKRAMWKDVLKKIGTVALHAGKAALGAVADTISQGEQ
DRS B2          MAFLKKSLFLVLFLGLVSLSICEEEKRENEDEEE--QEDDEQ---SEMKRGLWSKIKEVGKEAAKAAAKAAGKAALGAVSEAVGEQ
DRS B3          MAFLKKSVFLVLFLGLVSLSICEEEKREEENEEK--QEDDEQ---SEEKRALWKNMLKGIGKLAGQAALGAVKTLVGAE
DRS B4          MAFLKKSLFLVLFLGLVSLSICEEEKRENKDEIE--QEDDEQ---SEEKRALWKDILKNVGKAAGKAVLNTVTDMVNQGEQ
DRS B6          MAFLKKSLFLVLFLGLVSLSVCEEEKRENEDEME--QEDDEQ---SEEKRALWKDILKNAGKAALNEINQLVNQGEL
DRS G3          MAFLKKSLFLVLFLGLVSLSVCEEEKRENEDEEE--QEDDEQ---SEEKRALWKTIIKGAGKMIGSLAKNLLGSQAQPES
DRP-PBN1        MAFLKKSLFLVLFLGLVSLSICEEEKRETEEKEYDQGEDDK----SEEKRFLSLIPHIVSGVAALAKHLG
Dermatoxin      MAFLKKSLFLVLFLGLVPLSLCESEKREGENEEE--QEDD-Q---SEEKRSLGSFLKGVGTTLASVGKVVSDQFGKLLQAGQG
Phylloxin       MVFLKKSLLLVLFVGLVSLSICEENKRE-EHEEI--EENKE----AEEKRGWMSKIASGIGTFLSGMQQG
DRP-PD 1-5      MAFLKKSLFLVLFLGLVPLFLCENEKREGENEKE---ENDDQ---SEEKRSLGSFMKGVG-KGLATVGKIVADQFGKLLEAGKG
DRP-PD 2-2      MALVKKSLFLVLFLGLVSLSICE-EKRENEDEEE--QEDDEQ---SEEKRALWKTLLKKVGKVAGKAVLNAVTNMANQNEQ
DRP-PD 3-3      MAFLKKSLFLVLFLGLVSLSICE-EKRENEDEEE--QEDDEQ---SEEKRGMWSKIKNAGKAAAKASKKAAGKAALGAVSEALGEQ
DRP-PD 3-7      MSFMKKSLFLVLFLGVVSLSNCEEEKG-EENEEDH-EEHH------EEKRLLGDLLGQTSKLVNDLTDTVGSIV
DRP-AC3         MAFLKKSLLLVLFLGLVSLSICEEEKRENEDEEE--QEDDEQ---SEMRRSVLSTITDMAKAAGRAALNAITGLVNQGEQ
DRP-AA 1-1      MAFLKKSLFLVLFLGLVPLFLCENEKREGENEKE---ENDDQ---SEEKRSLGSFMKGVGKGLATVGKIVADQFGKLLEAGQG
DRP-AA 3-1      MAFLKKSLFLVLLLGLISLSICEEEKRENEVEEE--QEDDEQ---SELRRSLWSKIKEMAATAGKAALNAVTGMVNQGEQ
DRP-AA 3-3      MAFLKKSLFLVLFLGMVSLSICEEEKREEENE----QEDDEQ---SEEKRGMFTNMLKGIGKLAGQAALGAVKTLAGEQ
DRP-AA 3-4      MAFLKKSLFLVLFLGLVSLSICDEEKRENEDEEE--QEDDEQ---SEEKRGMWGSLLKGVATVVKHVLPHALSSQQS
DRP-AA 3-6      MAFLKKSLFLVLFLGLVSLSICEEEKRENEDEEE--QEDDEQ---SEMKRGMWSTIRNVGKSAAKAANLPAKAALGAISEAVGEQ
Caerin 1.1      MASLKKSLFLVLLLGFVSVSICEEEKR-QEDEDEHEEEGESQEEGSEEKRGLLSVLGSVAKHVLPHVVPVIAEHLG
Caerin 1.11     MASLKKSLFLVLFLGFVSVSICEEEKR-QEDEDEHEEEGENQEEGSEEKRGLFSVLGSVAKHVVPRVVPVIAEHLG
Caerin 1.12     MAFLKKSLFLVLFLGLVSLSICEEEKR-QEDEDEHEEEGENQEEGSEEKRGLFGILGSVAKHVLPHVVPVIAEHSG
Caerin 1.13     MASLKKSLFLVLFLGFVSVSICEEEKR-QEDEDENEEEGENQEEGSEEKRGLLSVLGSLKLIVPHVVPLIAEHLG
Caerin 1.14     MASLKKSLFLVLFLGFVSVSICEEEKR-QEDEDENEEEGENQEEGSEEKRSVLGKSVAKHLPHVVPVIAEKTG
Caerin 1.15     MASLKKSLFLVLFLGFVSVSICEEEKR-QEDEDENEEEGESQEEGSEEKRGLFGLAKGSVAKPHVVPVISQLVG
```

FIGURE 1: Nucleic acid and deduced amino acid sequences of cDNAs encoding Gly-Leu-rich peptides from the skin of *P. bicolor*, *P. dacnicolor*, *Agalycnis callidryas*, and *Agalycnis annae*. (A) Nucleic acid and predicted amino acid sequences of the cDNA encoding DRP-PBN2 (GenBank accession number AY218783). The predicted amino acid sequence is given in capital letters under the nucleotide sequence. The amino acid sequence of mature DRP-PBN2 is given in bold letters. The amino acid sequence of the signal peptide is underlined. Nucleotides and amino acids are numbered positively starting with position 1 of the open-reading frame. An asterisk indicates the stop codon. (B) Preprodermaseptins. The coding region, including the signal peptide, the acidic propiece, and the mature peptide progenitor sequences, is drawn as a rectangle. A comparison of the predicted amino acid sequences (single-letter code) of prepro-DRP-PBN2, prepro-DRP-PD 3−6 (*55*), prepro-DRP-AC1, prepro-DRP-AC2 (GenBank accession numbers AY218775 and AY218776), and prepro-DRP-AA 2−5 (*55*) to preprodermaseptins from South American and Australian hylid frogs. The predicted hydrophobic signal peptide includes the first 22 amino acid residues, while the acidic propiece (bold letters) comprises 21−27 residues. The mature peptide progenitor sequence is in italics. Gaps (−) have been introduced to maximize sequence similarities. Among the hylid sequences, DRS = dermaseptin B from *P. bicolor* and DRP = dermaseptin-related peptide (appended with AA, AC, or PD to indicate that the sequences were identified from *A. annae*, *A. callidryas*, and *P. dacnicolor*, respectively).

P. bicolor, *P. dacnicolor*, *A. callidryas*, and *A. annae*. Both methods indicate that DRP-PD 3−6, DRP-AA 2−5, DRP-AC1, DRP-AC2, and DRP-PBN2 are orthologs. The node indicating orthology with this clade is very well-supported with a bootstrap proportion of 100%, i.e., >95% confidence.

DRP-PBN2, DRP-AA 2−5, DRP-PD 3−6, DRP-AC1, and DRP-AC2 form a well-demarcated family of peptide orthologs with unique characteristics (Table 1). The putative peptides are rich in glycine and leucine (29 and 25% on average) arranged in regular 3-mer motifs GXL (where X is any other amino acid residue), which is repeated 2 (DRP-PBN2) to 5 (DRP-AA 2−5, DRP-AC1, and DRP-AC2) times. These Gly-Leu-rich putative peptides have fairly similar amino acid sequences (46−69% amino acid identity) with 10 invariant

Table 1[a]

DRP-AA 2-5	GLVSGLLNTAGGLLGDLLGSLGSLSGG*ES*	G...GXL...GXL.GXL.GXLGXL.G...
DRP-AC1	GLLSGILNTAGGLLGNLI---GSLSNG*ES*	GXL.GXL...GXL.GXL.---GXL.G...
DRP-AC2	GLLSGILNSAGGLLGNLI---GSLSNG*ES*	GXL.GXL...GXL.GXL.---GXL.G...
DRP-PBN2	GLVTSLIKGAGKLLGGLF---GSVTGGQS	G.....GXL.GXL.---G...G...
DRP-PD 3-6	GVVTDLLNTAGGLLGNLV---GSLSGG*ER*	G.....GXL.GXL.---GXL.G...

	1 5 10 15 20 25
DRP-PBN2	G L V T S L I K G A G K L L G G L F G S V T G G Q S
DRP-PBN2a	G L V T S L I K G A G K L L G G L F G S V T Ga
DRP-PD 3-6	G V V T D L L N T A G G L L G N L V G S L S Ga
ANC	G L V T G L L N T A G G L L G D L F G S L S Ga
[$K^{8,12}$]-ANC	G L V T G L L K T A G K L L G D L F G S L S Ga
[$K^{8,12}$]-DRP-PD 3-6	G V V T D L L K T A G K L L G N L V G S L S Ga
[$K^{8,12}$, F^{18}]-DRP-PD 3-6	G V V T D L L K T A G K L L G N L F G S L S Ga

[a] (Top) Comparison of the deduced amino acid progenitor sequence of the orthologous Gly-Leu-rich peptide from different species of hylid frogs (AA = *A. annae*, Ac = *A. callidryas*, PB = *P. bicolor*, and PD = *P. dacnicolor*). Alignments were performed by using CLUSTAL X Multiple Sequence Alignment software. Gaps (−) have been introduced to maximize sequence similarities. Identical amino acids are boldfaced. Amino acids in italics are removed during processing of proforms to expose the extra Gly residue (underlined), which serves as an amide donor for the C-terminal residue of DRP-PD 3−6, DRP-AC1, DRP-AC2, and DRP-AA 2−5. The progenitor sequences are arranged in regular 3-mer motifs GXL (where X is any of the 20 amino acid residues), which are repeated 2 (DRP-PBN2) to 5 (DRP-AA 2−5, DRP-AC1, and DRP-AC2) times. (Bottom) Amino acid sequence of the synthetic peptides investigated in this study. The amino acid sequence is in the standard one-letter code. a = amide. Identical amino acids are boldfaced.

residues (Gly[1], Ala[10], Gly[11], Leu[13], Leu[14], Gly[15], Leu[17], Gly[19], Ser[20], and Gly[24]). All substitutions involve replacement of an amino acid by one of similar polarity/hydrophobicity.

Tissue Distribution. The distribution of mRNA encoding DRP-PBN2 was examined by RT-PCR using specific oligonucleotide primers (see the Materials and Methods). A single amplification signal of the expected size was found in the skin, intestine, and brain (Figure 3). The purified PCR products were cloned in pGEM-Easy vector and sequenced to check that the amplified products correspond to DRP-PBN2 mRNA. Clones isolated from the intestine and brain have the same sequence as the skin DRP-PBN2, except for 2 silent base changes in the translated region of the former and 2 silent nucleotide changes in the latter (Figure 3).

Characterization of Gly-Leu-Rich Peptides from Skin Extracts. Predicted DRP-PD 3−6, DRP-AA 2−5, DRP-AC1, and DRP-AC2 have carboxytermini that end in the tripeptide G-E-S/R, which is similar to those of preprodermaseptins B1, B2, B4, and B6 (G-E-Q/L). As shown previously (*56*), removal of the dipeptide E-Q/L with carboxypeptidase or dipeptidylcarboxypeptidase during processing of the proforms exposes the extra Gly residue that serves as an amide donor for the C-terminal residue of the mature dermaseptins B. In contrast, the tripeptide ends of preprodermaseptin B3 (G-A-E) and preprodermatoxin (G-Q-G), which are similar to that of DRP-PBN2 (G-Q-S), are not involved in the formation of a C-terminal peptide amide (*56*). The skins of *P. bicolor* and *P. dacnicolor* were extracted with methanol/water and analyzed by reversed-phase HPLC to assess the status of the carboxyl terminus of DRP-PBN2 and DRP-PD 3−6 in vivo (Figure 4). The molecular masses of peptides in each chromatographic fraction were determined using MALDI−TOF mass spectrometry. Peaks from $m/z = 2000-4000$ Da were collected and purified by HPLC with a 20−80% linear gradient of acetonitrile in 0.1% TFA/water. The primary structures of the Gly-Leu-rich peptides detected (Table 1) were established by MS/MS fragmentation and de novo sequence analysis using a triple quadrupole nanoelectrospray tandem mass spectrometer (Figure 4). They showed that the native form of DRP-PD 3−6 contains 23 amino acid

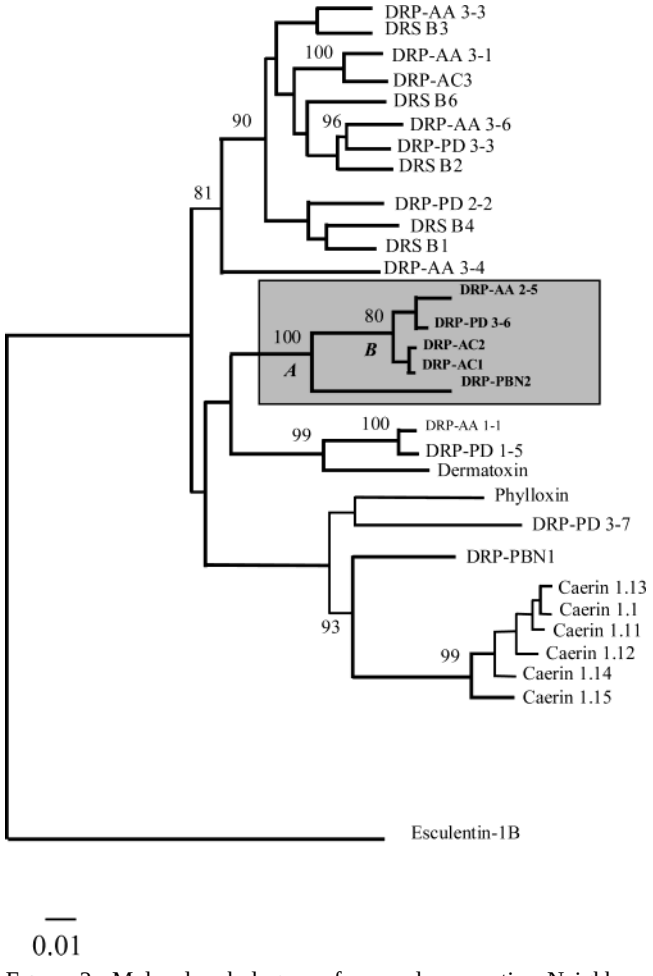

FIGURE 2: Molecular phylogeny of preprodermaseptins. Neighbor-joining tree constructed from Kimura two-parameter distances computed from a comparison of the entire preprodermaseptin cDNA sequences (including 3′- and 5′-untranslated regions) obtained from South American and Australian hylid and ranid frogs. Bootstrap values from 1000 replicates greater than 50% are indicated on branches. The distance scale is drawn below the tree. The phylogram is rooted with esculentin 1-B cDNA from *Rana esculenta* (*87*). Maximum-parsimony, maximum-likelihood, and LogDet analyses yielded the same ordinal phylogeny.

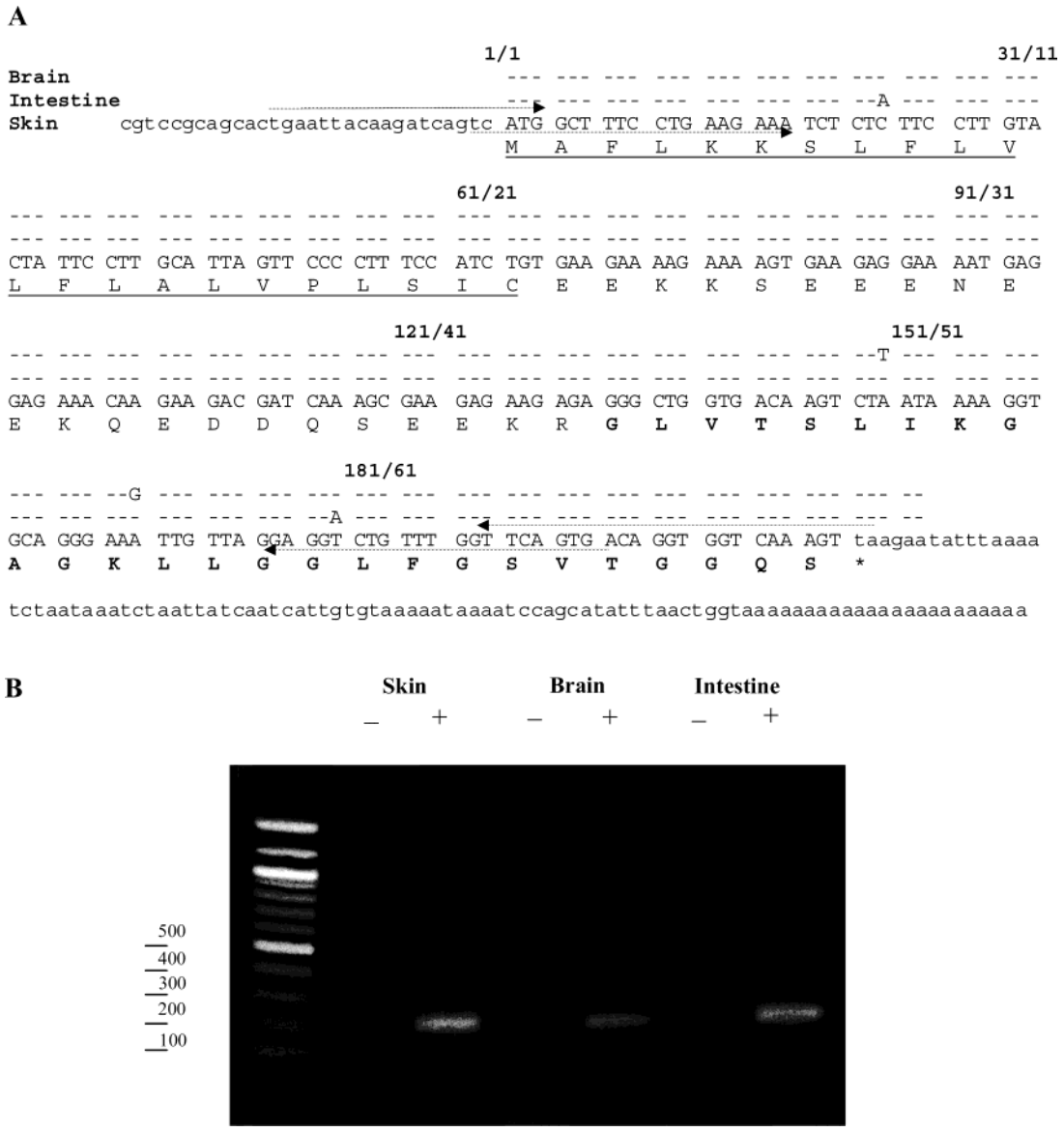

FIGURE 3: (A) Nucleic acid and deduced amino acid sequences of cDNAs encoding DRP-PBN2 from the skin, brain, and intestine of *P. bicolor*. The predicted amino acid sequence is given in capital letters above the nucleotide sequences. Nucleotides and amino acids are numbered starting with position 1 in the open-reading frames. Only nucleotides corresponding to differences between the brain and intestine DRP-PBN2 cDNAs and that of the skin are indicated. The amino acid sequence of mature DRP-PBN2 is in bold letters. The amino acid sequence of the signal peptide is underlined. Arrows indicate the sequence of the primers used. (B) Tissue distribution of mRNA for prepro-DRP-PBN2. Amplification products generated by RT-PCR from skin, brain, and intestine mRNAs were electrophoresed in 1.2% agarose gel.

residues with a carboxamidated C-terminal Gly residue. In contrast, no carboxamidated form of DRP-PBN2 was found. Because DRP-AA 2−5, DRP-AC1, and DRP-AC2 have carboxy termini that end in the tripeptide GES, it is thus very likely that mature DRP-AA 2−5, DRP-AC1, and DRP-AC2 are carboxamidated (Table 1).

Biological Studies of Cationic and Neutral Gly-Leu-Rich Peptides. DRP-PBN2 and DRP-PD 3−6 were used to determine whether structural differences between orthologous peptides from closely related frog species reflect differences of function. DRP-PBN2 and DRP-PD 3−6 differ by 10 amino acids (56% amino acid identity), but all of the amino acid differences have similar polarities. The peptides also differ in their net charge. DRP-PBN2 with a net charge of +2 (pI = 10), contains 2 positively charged lysine residues. These lysine residues are replaced by asparagine and glycine in DRP-PD 3−6 (pI = 5.5). An additional aspartate residue in position 5 of DRP-PD 3−6 generates a peptide with a net charge of 0. The 2 peptides have identical overall hydrophobicities (0.39) and amphipathicities, corresponding to a hydrophobic sector that subtends a radial angle of 180° on a helical wheel projection (Figure 5). Glycine residues are predominant within the polar surface of the helix of both molecules, while leucine is predominant on the nonpolar surface.

(A) Antimicrobial and Hemolytic Activities. The antimicrobial activities of DRP-PBN2 and DRP-PD 3−6 were assayed against Gram-negative and Gram-positive bacteria and yeasts (Table 2). Despite their orthologous relationships and similar sequences, their spectra of action differ considerably. Whereas DRP-PBN2 was active against most of the tested microorganisms at micromolar concentrations, DRP-PD 3−6 was virtually inactive. Bacteria incubated overnight with 25 μM DRP-PBN2 produced no colony-forming units,

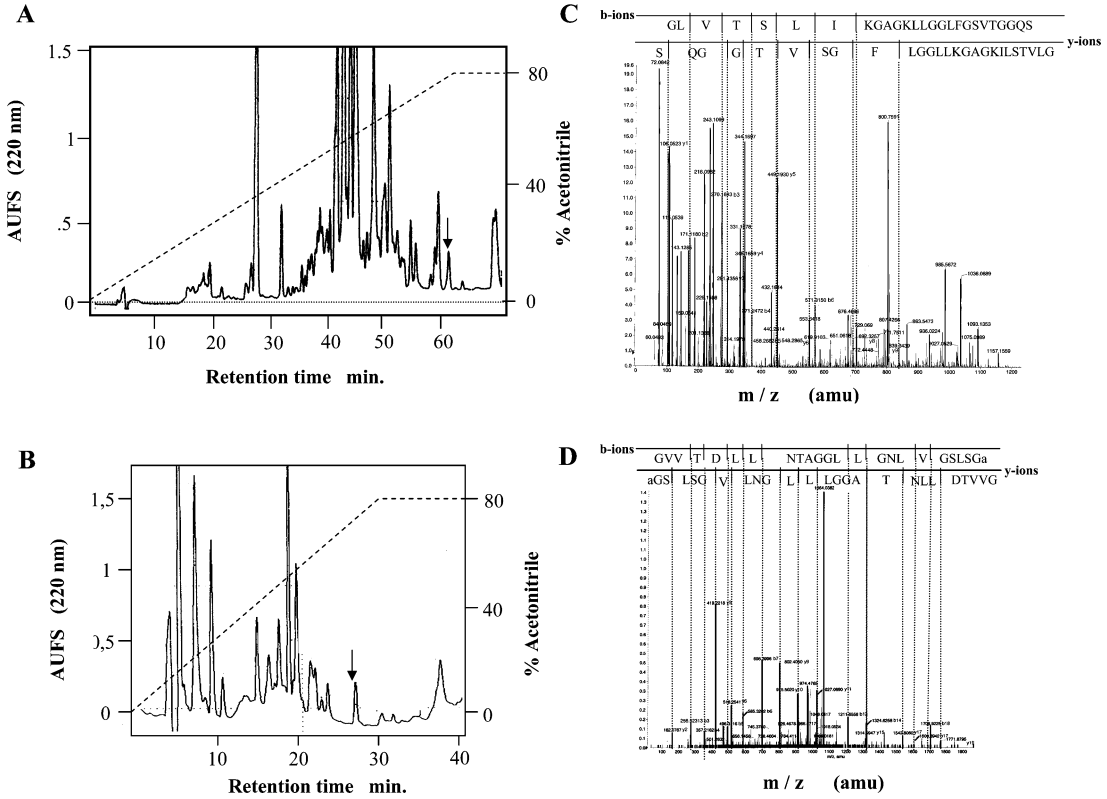

FIGURE 4: Purification of DRP-PBN2 and DRP-PD 3−6 from frog skin extracts and primary structure determination by nanoelectrospray tandem mass spectrometry. Dried extracts from the skin of (A) *P. bicolor* and (B) *P. dacnicolor* were dissolved in 0.1% TFA/water, applied to a Water RCM compact preparative cartridge Deltapak C 18 (100 × 25 mm), and eluted with a 20−80% linear gradient of acetonitrile containing 0.07% TFA at 0.75 mL/min. Absorption (—) was monitored at 220 nm. Fractions were lyophilized and analyzed by mass spectrometry. The arrows point to the elution positions of DRP-PBN2 and DRP-PD 3−6. (C) and (D) QTOF MS/MS fragmentation spectra and associated b- and y-ion sequence assignations of purified DRP-PBN2 and DRP-PD 3−6, respectively.

indicating that the peptide is bactericidal. Tests of the hemolytic activity of the peptides against rat erythrocytes (Table 2) showed that the 2 peptides have similar, albeit moderate, hemolytic activities.

(B) Kinetics of Bacterial Killing. The time taken by DRP-PBN2 to kill *E. coli* depended on the peptide concentration. At 48 μM, the peptide killed $\sim 2 \times 10^8$ cells mL^{-1} min^{-1}, with a total of 10^{10} cells/mL killed in 45 min (Figure 6). This rapid rate suggests that the membrane is the primary target of DRP-PBN2. Similar patterns were observed with other bacteria (not shown). DRP-PD 3−6 did not kill cells, even at the highest concentration used (47 μM).

(C) Permeabilization of the Bacterial Cytoplasmic Membrane. The disruption of the bacterial membrane by the peptides was detected by measuring the hydrolysis of the chromogenic substrate, ONPG, by the cytoplasmic β-galactosidase of *E. coli* K514 (wild type) after incubation with the peptides. DRP-PBN2 permeabilized the cytoplasmic membrane, as shown by the increasing release of enzyme with increasing concentrations of peptide, and ~100% enzyme activity even at the lowest peptide concentration was shown to cause bacterial death (Figure 6). These data again indicate that the bacterial membrane is one of the main targets of DRP-PBN2. In contrast, DRP-PD 3−6 did not result in β-galactosidase activity, showing that it does not permeate the bacterial membrane.

(D) Synergistic Effects. DRP-PBN1, FLSLIPHIVSGVAALAKHLG amide, from *P. bicolor*, is a member of the structurally diverse peptides encoded by the genes of the preprodermaseptin family. This peptide is active against only a few strains of Gram-positive bacteria (Table 2). DRP-PBN2 acts in a synergistic effect in combination with DRP-PBN1 (0.25 μM) at a dose that is not active alone, so that micromolar concentrations of the mixture had antibiotic activity against several strains of Gram-negative and Gram-positive bacteria. No synergistic effect was observed when DRP-PD 3−6 was used.

Biological Studies of Reconstructed Ancestral Sequence and Chimeric Peptides. We synthesized Gly-Leu-rich peptide analogues with altered net charges to determine whether cationicity combined with an amphipathic structure is sufficient to confer activity against microorganisms (Table 1). We also reconstructed and synthesized the ancestral peptide sequence from which extant DRP-PD 3−6, DRP-AA 2−5, DRP-AC1, and DRP-AC2 evolved to reveal the importance of amino acid substitutions in the functional divergence of these peptides and DRP-PBN2. All of the designed peptides had similar sizes, hydrophobicities, and amphipathicities, plus hydrophobic sectors that subtend 180° where they form an α-helical structure (Figure 5).

The sequence of the peptide ancestor (node B in Figure 2) of DRP-PD 3−6, DRP-AA 2−5, DRP-AC1, and DRP-AC2 was first inferred from the present-day sequences using parsimony and maximum-likelihood methods (see the Materials and Methods). The inferred ancestral peptide, ANC, was physicochemically more similar to DRP-PD 3−6 (82% identity) than to DRP-PBN2 (65% identity) (Table 1 and Figure 5). The four amino acid differences between DRP-PD 3−6 and its ancestor did not affect the net charge of the peptides (net charge = 0), their hemolytic activities, or their

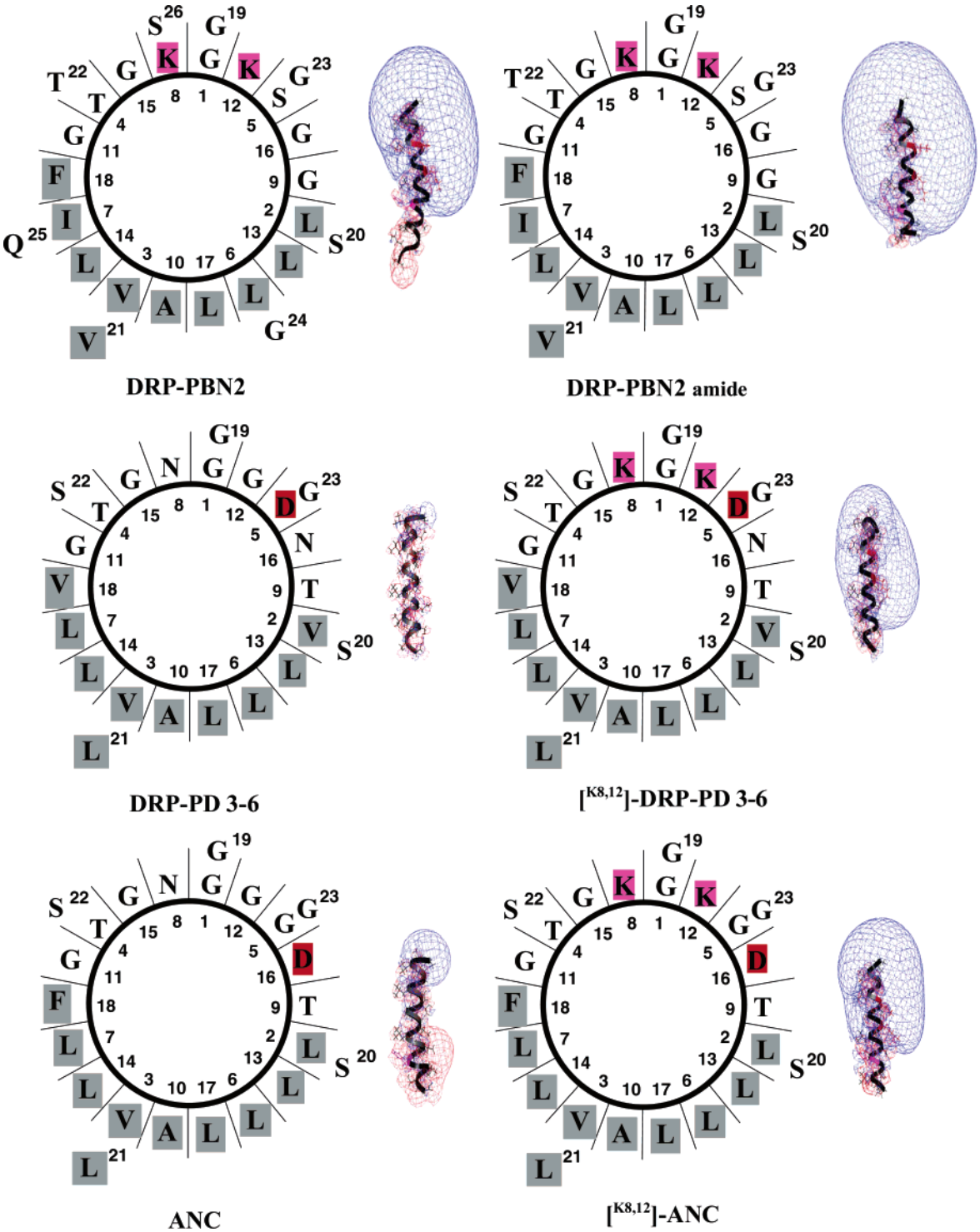

FIGURE 5: Amphipathic and electrostatic properties of Gly-Leu-rich peptides. Helical-wheel projections of the peptides demonstrate the amphipathic nature of the helices. Hydrophobic residues are shaded, and charged side chains are highlighted. The blue and red mesh represent the positive 1 kT/e and negative 1 kT/e electrostatic fields of the peptides calculated from the finite difference solution of the Poisson−Boltzmann equation.

antimicrobial potencies; both peptides were poorly active against only a few strains of bacteria (Table 2). The 8-residue differences between DRP-PBN2 and ANC include 3 that drastically alter the peptide net charge ($K^8 \rightarrow N$, $K^{12} \rightarrow G$, and $G^{16} \rightarrow D$). We therefore examined the role of Lys in positions 8 and 12 of DRP-PBN2 by changing Asn^8 and Gly^{12} in the ANC to Lys. This dramatically increased the antimicrobial activity (Table 2). The mutant peptide [K^8, K^{12}]-ANC (net charge = +2) was almost as potent as DRP-PBN2 against bacteria and yeasts. These findings provide experimental evidence that the gain of antimicrobial activity during the evolution of Gly-Leu-rich peptides was due to mutations altering charges. Similarly, increasing the net positive charge of DRP-PBN2 by one more units by carboxamidation of Gly^{23} resulted in a marked increase in antimicrobial activity (Table 2). Curves showing the killing of the *E. coli* strain by [K^8, K^{12}]-ANC showed that the time depended on the peptide concentration, similar as for DRP-

Table 2: Antimicrobial and Hemolytic Activities of Gly-Leu-Rich Peptides[a]

microorganisms		DRP-PBN2	DRP-PD 3-6	ANC [$K^{8,12}$]-ANC	DRP-PBN2a	[$K^{8,12}$]-DRP-PD 3-6	[$K^{8,12}$, F^{18}]-DRP-PD 3-6	DRP-PBN1	DRP-PBN2 + DRP-PBN1 (0.25 μm)
				Gram-Begative Bacteria					
Escherichia coli B	6.25	R[b]	R	25	6.25	12.5	12.5	R	6.2
Enterobacter cloacae	12.5	R	R	R	12.5	100	12.5	R	12.5
Klebsiella pneumoniae	6.25	R	R	12.5	3.1	100	6.25	R	nd[c]
Salmonella enteritidis	3.1	R	R	6.25	1.5	25	3.1	R	nd
Clostridium perfringens	50	R	R	R	25	nd	100	R	1.5
Listeria monocytogenes	25	R	R	R	12.5	nd	50	R	nd
Neisseria meningitidis	50	R	R	25	25	100	50	R	1.5
Vibrio cholerae	25	R	R	12.5	6.25	25	25	R	6.2
Pseudomonas aeruginosa	3.1	R	R	50	1.5	100	3.1	R	nd
Salmonella typhimurium	3.1	R	nd	3.1	6.25	50	6.25	R	25
				Gram-Positive Bacteria					
Staphylococcus haemolyticus	50	300	400	25	6.25	100	50	R	3.1
Staphylococcus aureus	6.25	250	300	12.5	6.25	50	6.25	12.5	1.5
Streptococcus pneumoniae	6.25	nd	nd	3.1	3.1	nd	12.5	R	nd
Bacillus megaterium	25	R	R	12.5	3.1	12.5	50	3.1	0.4
Burkholderia cepacia	R	R	R	R	R	R	R	R	R
				Yeasts					
Candida albicans	50	R	nd	50	12.5	150	50	nd	nd
Saccaromyces cerevisiae	50	R	nd	100	12.5	300	100	nd	nd
% hemolysis at 50 μM	30	42	43	22	nd	35	nd	nd	nd
% hemolysis at 100 μM	70	75	65	48	nd	71	nd	nd	nd

[a] Antimicrobial activity is expressed as MIC (μM), the minimal peptide concentration required for the total inhibition of cell growth in liquid medium. Results are the mean of three independent experiments, each performed in duplicate with the standard deviation not exceeding 15%. [b] Strains were considered resistant (R) when their growth was not inhibited by peptide concentrations up to 400 μM. [c] Not determined.

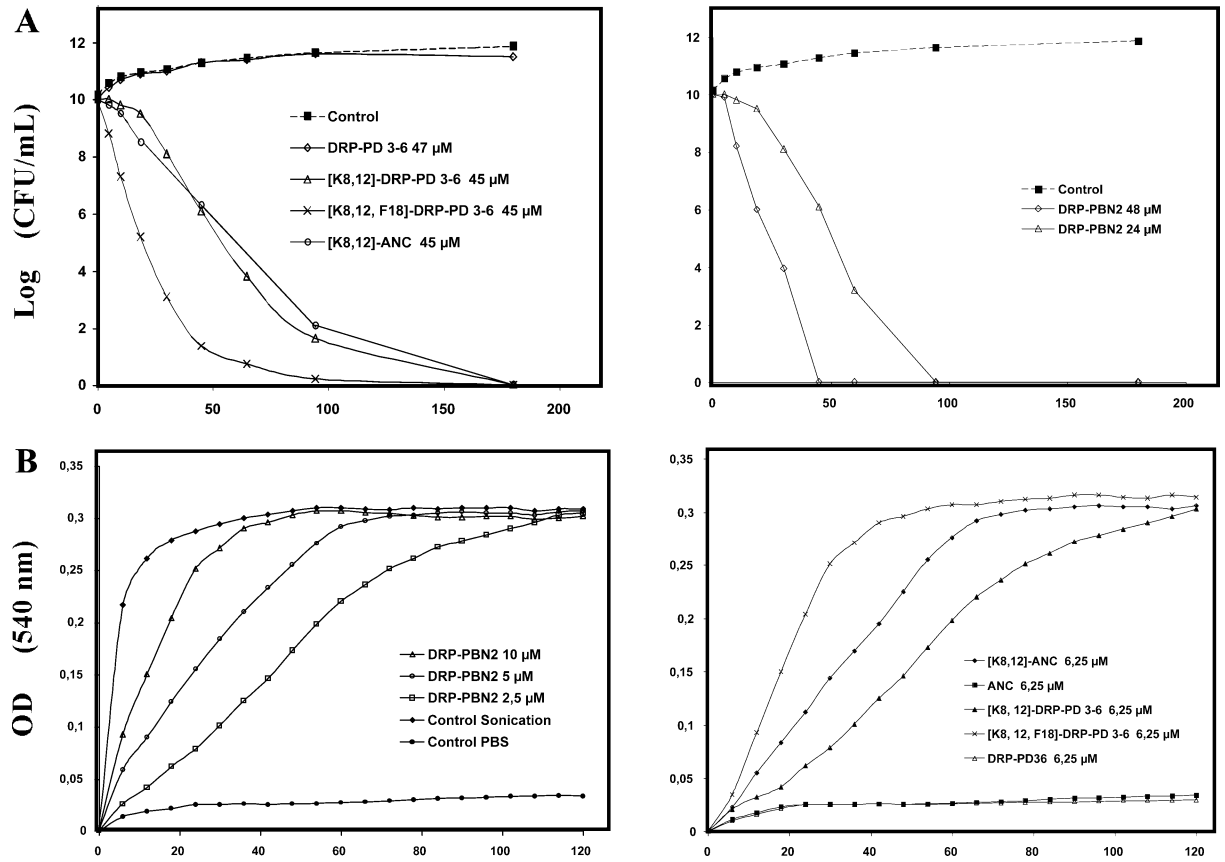

FIGURE 6: Kinetics of bactericidal action and bacterial membrane permeabilization. (A) In vitro time-killing curves of two concentrations of DRP-PBN2 (right panel) and a single concentration of [K^8, K^{12}]-ANC, [K^8, K^{12}]-DRP-PD 3−6, [K^8, K^{12}, F^{18}]-DRP-PD 3−6, and DRP-PD 3−6 (left panel) against *E. coli*. The data are expressed as bacterial-colony-forming units per milliliter of culture medium (CFU/mL), as a function of the incubation time with the peptide (see the Materials and Methods). (B) Kinetics of the cytoplasmic membrane leakage of *E. coli* after treatment with increasing concentrations of DRP-PBN2 (left panel) and with 6.25 μM of [K^8, K^{12}]-ANC, [K^8, K^{12}]-DRP-PD 3−6, [K^8, K^{12}, F^{18}]-DRP-PD 3−6, ANC, and DRP-PD 3−6 (right panel). The membrane leakage was followed by measuring the hydrolysis of ONPG at 540 nm by the cytoplasmic bacterial β-galactosidase in the filtrate of the *E. coli* culture after incubation with the peptides (see the Materials and Methods).

PBN2 (Figure 6). ANC showed no killing activity, even at the highest concentration used (40 μM). [K^8, K^{12}]-ANC also permeabilized membranes with almost the same activity as DRP-PBN2 (Figure 6). Thus, the microbicidal activity seems to depend on the overall cationic charge density of the polar helix surface.

We checked this by introducing lysine residues at positions 8 and 12 of DRP-PD 3−6 to give a peptide with charge +2. The time-killing curves and membrane permeabilizing activity of [K^8, K^{12}]-DRP-PD 3−6 were similar to those of [K^8, K^{12}]-ANC (net charge = +2) (Figure 6). However, it was a less potent antibiotic than [K^8, K^{12}]-ANC (Table 2), indicating that the 2 lysine residues are necessary but not sufficient for broad-spectrum antimicrobial activity. The 5 amino acid differences between [K^8, K^{12}]-ANC and [K^8, K^{12}]-DRP-PD 3−6 include two that alter charge (G^5 → D and D^{16} → N) but are compensatory, because they produce no difference in the net charges of the peptides. The Val^{18} in [K^8, K^{12}]-DRP-PD 3−6 was replaced by Phe because there is a Phe at position 18 in [K^8, K^{12}]-ANC and DRP-PBN2 and aromatic residues are especially favored at the interfaces of phospholipid membranes. This change improved its antimicrobial activity, making it similar to that of DRP-PBN2 and [K^8, K^{12}]-ANC (Table 2 and Figure 6). This suggests that an aromatic residue in that position confers broad-spectrum antimicrobial activity to Gly-Leu-rich peptides.

Mode of Action Studies with Model Membranes. The neutral Gly-Leu-rich peptides may be unable to kill microorganisms because they cannot bind to anionic phospholipid membranes or, if they are bound, cannot organize themselves into structures that lyse the membrane. We investigated the interactions of peptides with model bilayers by CD spectroscopy and SPR to distinguish between these possibilities. DMPG was chosen as a model system for the membrane of bacteria because their outer leaflets are composed largely of anionic phospholipids. DMPC, a zwitterionic phospholipid, was used as a model for mammalian cell membranes.

(A) Secondary Structure of the Peptides Determined by CD Spectroscopy. The CD spectra resulting from titration of 30 μM aqueous solutions of DRP-PBN2, [K^8, K^{12}]-ANC, [K^8, K^{12}]-DRP-PD 3−6, and [K^8, K^{12}, F^{18}]-DRP-PD 3−6 by zwitterionic DMPC or anionic DMPG vesicles (Figure 7) showed that the cationic peptides have very little ordered structure in aqueous solution except for [K^8, K^{12}, F^{18}]-DRP-PD 3−6, which has ∼20% helix. The same peptides had helical-ordered structures with the characteristic minima at 208 and 222 nm when mixed with DMPC or DMPG vesicles. The secondary structure produced using the consensus prediction at the Network Protein Sequence Analysis web server (*72*) indicate that the helical structure is within the central region (from residues 3−4 to 15−18) of the peptides. The effect of anionic lipids on peptide conformation was concentration-dependent, saturating at ∼500 μM DMPG (lipid−peptide ratio of 17) or ∼2700 peptide molecules/vesicle, assuming 44 000 DMPG molecules/vesicle. More lipid produced no further changes in the CD spectra, suggesting that the peptides are completely associated with the vesicles. The rank order of peptide helix contents was [K^8, K^{12}]-ANC (42% helix) < DRP-PBN2 (45% helix) < [K^8, K^{12}, F^{18}]-DRP-PD 3−6 (50% helix) < [K^8, K^{12}]-DRP-PD 3−6 (52% helix) in the presence of DMPC vesicles and [K^8, K^{12}]-ANC (35% helix) < DRP-PBN2 (40% helix) < [K^8, K^{12}, F^{18}]-DRP-PD 3−6 (50% helix) < [K^8, K^{12}]-DRP-PD 3−6 (55% helix) in the presence of DMPG vesicles. Similar helix contents and identical rank orders of helix contents were found with DMPC and DMPG vesicles. Thus, once a cationic peptide is bound to a zwitterionic lipid bilayer, it adopts the same secondary structure as a negatively charged bilayer. DRP-PD 3−6 and ANC, which have no net charge, interact with DMPG vesicles and adopt a helical structure (55 and 30% helical contents) (Figure 7). Because the partitioning of these peptides into DMPG vesicles can be accounted for solely by their hydrophobicity, hydrophobic effects should account for the binding capacity of the neutral peptides to anionic lipids. This stresses the importance of hydrophobic interactions between the peptides and the lipid bilayer for helix formation and stabilization. However, the observation that cationic peptides have a maximum helicity at lower lipid/peptide ratios of PG than PC suggests that basic peptides interact best with anionic lipid vesicles and worse with zwitterionic vesicles. This provides direct evidence that the hydrophobic nature of the cationic peptides in concert with their positive net charge provide increased affinity and selectivity for negatively charged bilayers via Coulombic interactions.

The CD spectra obtained by titrating 30 μM aqueous solutions of DRP-PD 3−6 with zwitterionic DMPC vesicles showed a broad minimum around 220 nm, suggesting the presence of a mixture of β structures. The fact that the structure of DRP-PD 3−6 differs widely in the presence of anionic and neutral vesicles demonstrates that this peptide has "chameleon-like" properties at biomembrane surfaces; i.e., the same amino acid sequence can have several conformations, depending almost exclusively on the molecular environment. Other studies have shown similar interconversions between α helices and β sheets modulated by the molecular environment (*73*).

Bacterial surfaces contain lipopolysaccharides (LPS, in Gram-negative bacteria) and polysaccharides (teichoic acids, in Gram-positive bacteria) as well as phosphatidylglycerol in their cytoplasmic membrane, all of which are negatively charged. Cationic Gly-Leu-rich peptides combine an α-helical structure with strong antibacterial activity and moderate hemolytic activity. In contrast, DRP-PD 3−6 and ANC, which have no net charge and little or no antimicrobial activity, adopt an α-helical structure when bound to anionic vesicles but are predominantly nonhelical in the presence of neutral vesicles. Thus, an amphipathic helical structure is not sufficient, in this case, for bacterial membrane disruption. It also suggests that hemolytic activity does not require, except for a high hydrophobicity, a defined structure such an α helix or a positive net charge.

Gly-Leu-rich peptides and their analogues contain 7−8 glycine residues (α-helix breakers) and 3−5 valine/threonine residues (β-sheet promoters). Glycine introduces flexibility and enables solvents to get close to the peptide backbone, thereby preventing these peptides from forming ordered structures in water. Nevertheless, all of these peptides have similar helical content in DMPG vesicles, regardless of their different primary structures. This shows that these residues can be incorporated as readily as Leu or Ala into a helix in a membrane-interfacial environment and that the propensity of a peptide to form a helix is specified by the

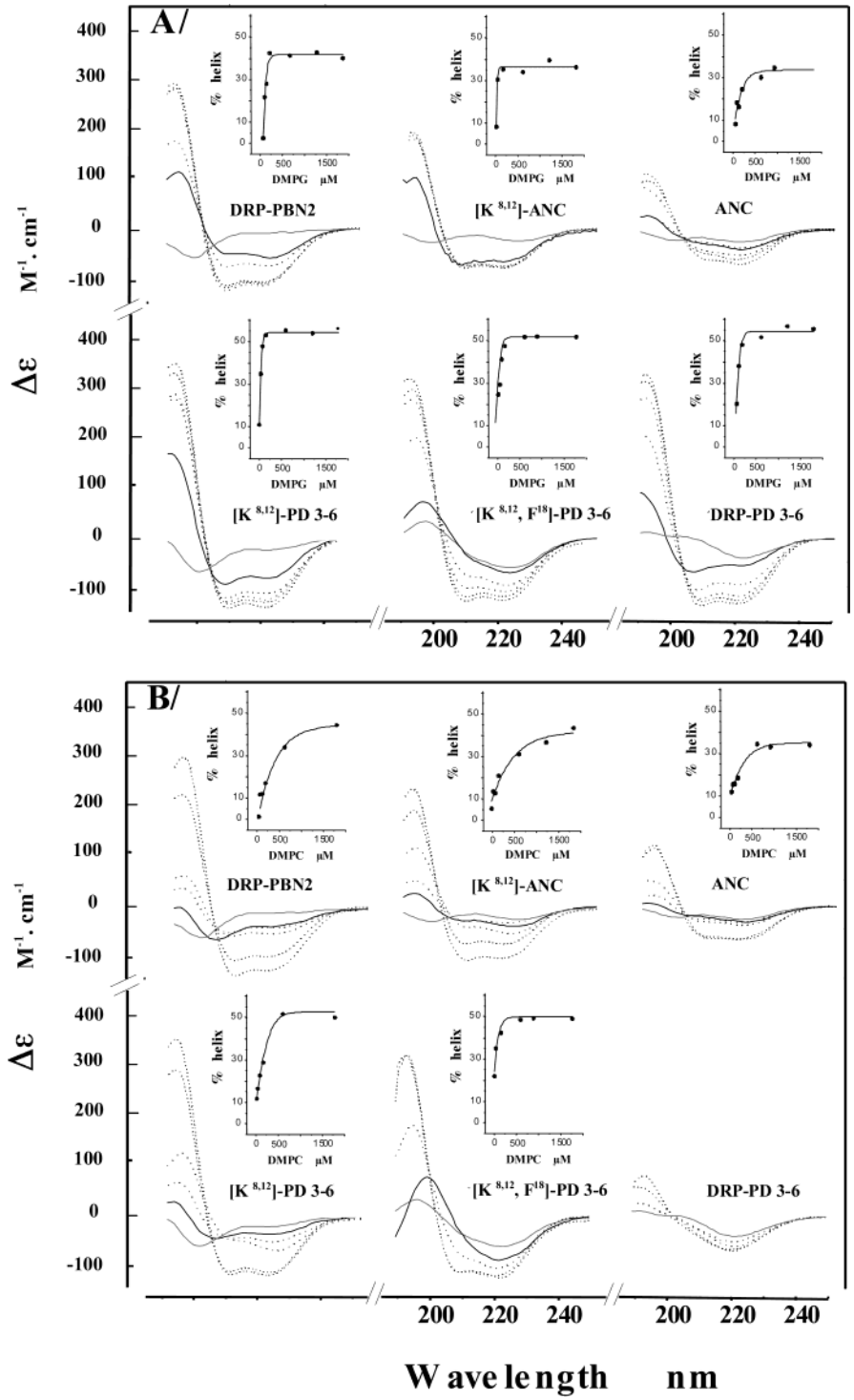

FIGURE 7: Secondary structure of Gly-Leu-rich peptides. CD spectra of Gly-Leu-rich peptides in the presence of increasing concentrations of (A) anionic DMPG LUVs and (B) zwitterionic DMPC LUVs in a phosphate buffer at pH 7 plus 150 mM NaCl. The phospholipid concentrations used were 0, 30, 75, 150, 600, and 1800 μM. The curves with a higher intensity correspond to the higher phospholipid concentrations. The peptide concentration was held constant at 30 μM for all measurements. The inserts show the dependence of the percentage of α-helical structure in peptides on the concentration of DMPG and DMPC vesicles.

environment (*74*). It is also possible that the intrinsic flexibility of several Gly residues is hindered by neighboring bulky Leu residues.

(B) Binding to Lipid Bilayers as Measured by SPR. The affinity of antimicrobial peptides for phospholipid surfaces is a critical factor influencing their selectivity and potency but is not commonly measured and reported. We have used a new, sensitive method based on SPR to make real-time measurements of the peptide binding to phospholipid membranes. The sensorgrams for the binding of DRP-PBN2, [K^8, K^{12}]-ANC, [K^8, K^{12}]-DRP-PD 3−6, [K^8, K^{12}, F^{18}]-DRP-PD 3−6, ANC, and DRP-PD 3−6 to immobilized planar bilayers of anionic DMPG or zwitterionic DMPC are shown in Figure 8, together with typical sensorgrams for various concentrations of DRP-PBN2 with DMPG and DMPC bilayers. The binding of the peptides to both lipids increased with the peptide concentration until the system was saturated. This indicates specific interactions between the peptides and the

Table 3: Equilibrium Affinity Constants and Association [k_{A1} (M^{-1} s^{-1}) and k_{A2} (s^{-1})] and Dissociation [k_{D1} (s^{-1}) and k_{D2} (s^{-1})] Rate Constants of the Peptides with DMPG and DMPG Bilayers (L1 Chips) Determined by Numerical Integration Using the 2-State Model[a]

	DRP-PBN2	[$K^{8,12}$]-ANC	DRP-PD 3−6	[$K^{8,12}$]-DRP-PD 3−6	[$K^{8,12}$ F^{18}]-DRP-PD 3−6
			DMPC		
k_{a1} (M^{-1} s^{-1})	7.6×10^3	2.2×10^3	3.3×10^0	1.2×10^4	1.0×10^4
k_{d1} (s^{-1})	4.0×10^{-2}	2.7×10^{-2}	9.0×10^{-3}	4.8×10^{-2}	3.0×10^{-2}
k_{a2} (s^{-1})	6.9×10^{-3}	7.7×10^{-3}	6.0×10^{-3}	6.4×10^{-3}	6.4×10^{-3}
k_{d2} (s^{-1})	8.0×10^{-4}	7.2×10^{-4}	2.0×10^{-5}	1.1×10^{-3}	1.8×10^{-3}
K_{A1}	1.9×10^5	0.8×10^5	3.7×10^2	2.5×10^5	3.3×10^5
K_{A2} (M^{-1})	8.6×10^0	11.0×10^0	3.0×10^2	5.8×10^0	3.5×10^0
K_A (M^{-1})	**1.6×10^6**	**0.9×10^6**	**1.1×10^5**	**1.4×10^6**	**1.1×10^6**
			DMPG		
k_{a1} (M^{-1} s^{-1})	6.0×10^3	4.2×10^3	nd[b]	1.6×10^4	2.1×10^3
k_{d1} (s^{-1})	1.0×10^{-2}	6.8×10^{-3}	nd	4.6×10^{-3}	2.0×10^{-2}
k_{a2} (s^{-1})	3.8×10^{-3}	5.4×10^{-3}	nd	1.3×10^{-3}	4.2×10^{-3}
k_{d2} (s^{-1})	1.2×10^{-6}	2.8×10^{-6}	nd	3.5×10^{-5}	2.1×10^{-6}
K_{A1}	6.0×10^5	6.1×10^5	nd	3.5×10^6	1.0×10^5
K_{A2} (M^{-1})	3.1×10^3	1.9×10^3	nd	3.7×10^1	2.0×10^3
K_A (M^{-1})	**1.9×10^9**	**1.2×10^9**	**nd**	**1.3×10^8**	**2.0×10^8**

[a] Affinity constants K_{A1} (M^{-1}) and K_{A2} (unitless) are for the first ($K_{A1} = k_{a1}/k_{d1}$) and second ($K_{A2} = k_{a2}/k_{d2}$) steps, respectively, and the affinity constant (K_A) determined as (k_{a1}/k_{d1}) × (k_{a2}/k_{d2}) is for the complete binding process. [b] Not determined (see the Results).

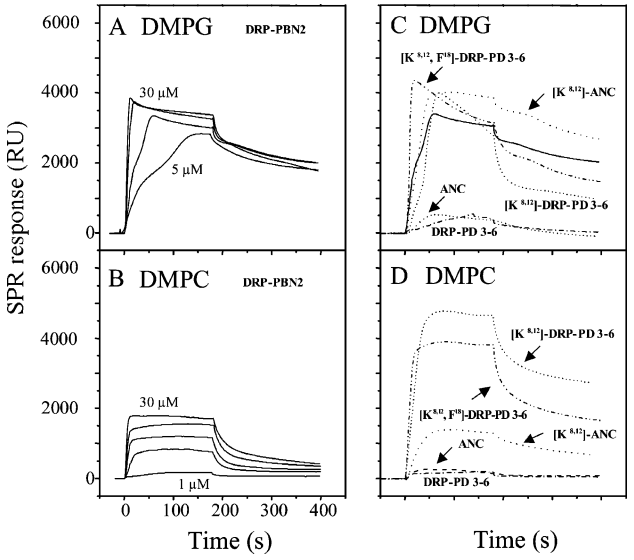

FIGURE 8: SPR sensorgrams of the binding of various concentrations of DRP-PBN2 and the lipid bilayer (L1 chip) with (A) DMPG and (B) DMPC at pH 7. Peptide concentrations used are 1, 5, 10, 20, and 30 μM. Injections were made at time = 0 min, and PBS was added to initiate dissociation at 180 s. The curves with a greater intensity correspond to the higher peptide concentrations. Sensorgrams for 10 μM [K^8, K^{12}]-ANC, [K^8, K^{12}]-DRP-PD 3−6, [K^8, K^{12}, F^{18}]-DRP-PD 3−6, ANC, and DRP-PD 3−6 binding to (C) zwitterionic DMPG and (D) anionic DMPC bilayers immobilized on the L1 sensor chip surface.

bilayers. The shapes of the sensorgrams revealed different binding kinetics with significant differences in the association and dissociation rates for both lipid surfaces. The initial association and dissociation of the cationic peptides with both lipid surfaces was very rapid and then slowed. The sensorgrams for most peptides did not return to zero following dissociation, indicating that some peptides remained bound to the lipid or inserted into the lipid bilayer. Linearization and curve fitting using numerical integration were used to obtain the association (k_a) and dissociation (k_d) rate constants. The 1:1 binding models with or without mass transfer limitation, bivalent analyte, or heterogeneous ligand models produced very poor fits, indicating that they are not appropriate for the complex peptide−membrane interaction. The sensorgram curves were fitted to a 2-state model using BIA evaluation 3.0 software (eqs 1−4) where P is the analyte

$$\mathrm{P} + \mathrm{L} \underset{k_{d1}}{\overset{k_{a1}}{\leftrightarrow}} \mathrm{PL} \underset{k_{d2}}{\overset{k_{a2}}{\leftrightarrow}} \mathrm{PL}^* \quad (1)$$

$$\mathrm{d[PL]/d}\,t = k_{a1}C_p[R_{max} - R] - k_{d1}[\mathrm{PL}] - k_{a2}[\mathrm{PL}] + k_{d2}[\mathrm{PL}^*] \quad (2)$$

$$\mathrm{d[PL^*]/d}\,t = k_{a2}[\mathrm{PL}] - k_{d2}[\mathrm{PL}]^* \quad (3)$$

$$k_{a1}/k_{d1} \times k_{a2}/k_{d2} = K_A \quad (4)$$

(peptide), L is the immobilized membrane, PL is the initial complex formed by the lipid membrane and peptide, and PL* is the lipid−peptide complex. This complex cannot dissociate directly to P + L and may correspond to a structural/conformational change in PL that leads to a more stable complex PL*. R_{max} is the maximum signal in RU, which is proportional to the initial concentration of lipids, R is the signal in RU from the biosensor, which is proportional to the total amount of complex PL + PL*, and C_p is the peptide concentration. Because this model fitted the experimental data well, it may correctly portray the interaction of antimicrobial peptides with bilayers as a 2-stage process, with initial surface adsorption, followed by insertion of the peptide into the membrane interior, leading to disruption of the bilayer once a critical concentration is reached or interaction between free and membrane-bound peptides to form transmembrane pores. The second stage may involve a conformational change in the peptide−membrane complex to increase the stability of the complex. The sensorgrams of the binding of DRP-PD 3−6 and ANC to DMPG indicate poor responses and dissociation at peptide concentrations up to 30 μM and only a barely detectable response at concentrations below 10 μM (Figure 8). As a consequence, no values for the rates of association and dissociation in the first and second stages of the interaction were determined. The fact that DRP-PD 3−6 and ANC are helical in the presence of DMPG vesicles (Figure 7) but bind poorly to immobilized DMPG bilayers is probably due to their different morphologies. The curvature of the vesicles exposes the hydrophobic

core of the lipid bilayer more than in the planar anionic membrane immobilized on the sensor.

Table 3 shows the overall equilibrium constant, K_A, for the binding of peptides to both zwitterionic and negatively charged membranes. The cationic peptides bind to both anionic and zwitterionic phospholipids membranes, but their affinity for anionic membranes is 100−1000-fold greater than that for the zwitterionic membranes. This indicates that electrostatic interactions are important for their affinity for membranes. The cationic peptides have similar, low affinities for zwitterionic membranes. This may partially explain the low hemolytic activity of the basic peptides compared to their high antibacterial potency. [$K^{8,12}$]-ANC contains a negative charge (Asp^{16}), which may counteract the hydrophobic driving force by electrostatic repulsion with the anionic membrane surface. The negatively charged aspartate group may also prevent the peptides from penetrating into the hydrophobic region of the bilayer. However, this peptide binds to the anionic membrane as strongly as DRP-PBN2. According to Johnson et al. (*75*), we proposed that anionic vesicles have a negative surface potential that lowers the surface pH, thus increasing the proton concentration at the membrane surface. This would increase the probability of protonation (increasing the apparent pK_a) and charge neutralization of the aspartate residue close to the surface of a negatively charged membrane more than that for a zwitterionic membrane, enhancing the hydrophobicity of the peptides. Hence, the aspartate residue could enhance the selectivity of the peptides for anionic phospholipids.

These findings may suggest that long-range Coulombic attractions between positively charged peptides and negatively charged headgroups of the anionic membrane increase the selectivity for anionic membranes by increasing the concentration of the peptide in the vicinity of the membrane surface to a threshold peptide−lipid molar ratio, leading to membrane disruption. The free energy of the hydrophobic binding of DRP-PBN2 is $\Delta G \sim -8.7$ kcal/mol, as deduced from its binding to zwitterionic bilayers. This corresponds to the hydrophobic stabilization of the α helix by interactions of the nonpolar surface of the helix with the acyl chains of the lipids implying the transfer of 10 nonpolar side chains from aqueous to nonpolar membrane environments. Because the difference in K_A for the binding of DRP-PBN2 for DMPG is ∼1000-fold greater than its binding to DMPC and the free energies of hydrophobic and electrostatic interactions are additive, electrostatic interactions contribute an additional 4.2 kcal/mol to the free energy of binding. Even though the contribution of electrostatic forces to the overall affinity-binding constant seems modest, it could result in 1000-times more peptide in the vicinity of the anionic membrane surface than in the bulk peptide solution. Because cationic peptides have a much lower binding affinity for zwitterionic membranes than for anionic membranes, higher concentrations are needed to reach the threshold concentration for rupture of zwitterionic membranes. This may be why both cationic and neutral Gly-Leu-rich peptides have low cytotoxicity for erythrocytes.

We next determined exactly how electrostatic and hydrophobic interactions influence the membrane-binding properties of cationic Gly-Leu-rich peptides by analyzing the rate constants for the 2-state model along with the individual affinity constants K_{A1} and K_{A2} of each stages of the interaction (Table 3). K_{A1}, the first stage association affinity constant, indicates the adsorption of the peptide to the membrane surface (primary binding), whereas K_{A2} is unitless and reflects the tendency of the peptide to become inserted into or to assemble on the membrane and subsequently move from the surface to become inserted. The main observations were that the first stage rates of association (k_{a1}) and dissociation (k_{d1}) for the interaction with DMPG and DMPC are similar, indicating that electrostatic interactions are not important for the initial binding of the cationic peptides to anionic membranes. Therefore, the first step is mainly governed by hydrophobic interactions between the peptides and the membranes. Second, the second stage rates of association (k_{a2}) with both DMPC and DMPG are similar, indicating that the peptides have similar rates of insertion into the anionic and zwitterionic membranes. Third, the difference between binding to DMPG and DMPC is the result of the second step and not the first step. This is because cationic peptides dissociate ∼100−1000-times more slowly (k_{d2}) from DMPG than from DMPC in the second step, but they have similar rate constants k_{a2} for binding to DMPG and DMPC. This indicates that short-range ionic interactions are important for stabilizing the peptide inserted into the anionic membrane; i.e., once the peptide is bound to the membrane, it is practically "glued" into the acyl region of the membrane in a quasi-irreversible fashion, with little or no release. This suggests that short-range Coulombic interactions between the positively charged lysine residues of the inserted peptides and the negatively charged headgroups of the phospholipids anchor the peptide to the membrane through snorkeling of the lysine side chains lying at the polar helix surface (*76*). Unlike the mutations of ionic residues that primarily affect K_{A2} for anionic membranes, our SPR analysis shows that the substitution of Val^{18} for Phe in [K^8, K^{12}]-DRP-PD 3−6 influences both K_{A2} and K_{A1}, although the change in K_{A2} was much larger than that in K_{A1}. This demonstrates that the aromatic side chain plays a complex role in interfacial binding, in addition to prolonging the membrane residence time of the inserted peptide. Thus, the binding of Gly-Leu-rich cationic peptides to anionic membranes is driven first by the hydrophobic interactions and then by short-range ionic interactions. There is also no correlation between the K_{A1} for anionic membranes and antimicrobial activity, whereas there is a rough correlation with K_{A2}. Hence, the antimicrobial potency of cationic Gly-Leu-rich peptides is not due to their high adsorption affinity (K_{A1}) for anionic membranes but to their great propensity to become locked into the acyl region of the anionic membranes.

We propose a general model for the binding of cationic Gly-Leu-rich peptides to anionic membranes. The cationic peptide initially binds to the membrane surface because of the hydrophobic effect and several nonspecific noncovalent interactions, leading to an ensemble of peptides loosely bound to the membrane. The subsequent formation and adjustment of the peptide helix result in tightly bound peptide−membrane complexes that are primarily stabilized by the peptide aliphatic and aromatic residues penetrating deep into the membrane, together with short-range Coulombic interactions between the lysine residues of the peptide and the anionic headgroups of the phospholipids. The behavior of cationic Gly-Leu-rich peptides is significantly

different from that of the small membrane-damaging cationic peptides magainins and dermaseptins, which were studied recently using SPR technology (*77*−*80*). Magainins and dermaseptins are Lysine-rich α-helical amphipathic peptides that have broad-spectrum antimicrobial activity but are not very toxic for mammalian cells. These peptides also have low hydrophobicity and flexibility (*41*, *44*, *81*, *82*) and interact with anionic lipids ∼100 times better than with zwitterionic lipids. However, this difference in binding is mainly due to the first binding step that is governed by nonspecific long-range electrostatic interactions between the peptide lysine residues and the anionic headgroups of the phospholipids. In contrast, the affinity constants for the second binding step, K_{A2}, for anionic and zwitterionic membranes are similar, indicating that electrostatic interactions are not important for the insertion of the peptide into the membrane and its stabilization. Our results indicate that Gly-Leu-rich peptides are clearly different from magainins and dermaseptins; selection of the target membranes by Gly-Leu-rich peptides takes place in the second binding step. The lysine residues of Gly-Leu-rich peptides specifically stabilize the peptide−membrane complex once the peptide is inserted into the membrane. Although the details of the mechanisms by which cationic Gly-Leu-rich peptides permeate and disrupt bacterial membranes are still unknown, the equilibrium constants of the second binding step resemble those of peptides that become inserted deep into the hydrophobic core of the membrane or form transmembrane pores, rather than lying on the outer surface (*77*−*79*).

Evolution of the Antimicrobial Activity of Gly-Leu-Rich Peptides. The branch giving rise to DRP-PBN2 in *P. bicolor* (potent antimicrobial activity and low hemolytic activity) developed very different properties from ANC, the ancestor of DRP-PD 3−6 in *P. dacnicolor* (no antimicrobial activity and low hemolytic potency), 60−100 million years ago. This change in function mainly relies on two (Asn^8 → Lys and Gly^{12} → Lys) of the eight amino acid differences between the two peptide sequences, affecting the net charge of the peptides and their ability to bind to and permabilize bacterial membranes. The evolutionary divergence of species usually results in orthologous variants of the same protein, all with the same three-dimensional structure and biological function but different amino acid sequences. The functional constraints of orthologous proteins usually remain the same so that Dn/Ds, the ratio of nucleotide nonsynonymous substitutions (amino acid altering substitutions) per nonsynonymous sites to nucleotide synonymous substitutions (silent substitutions) per synonymous sites, is usually a constant, low value ($\ll 1$). Major deviation from this rule can occur if the diverging species adapt to different environments and the function of the encoded proteins is altered. During such adaptations, there is a positive (Darwinian) selection for advantageous mutations that make the protein better adjusted so that Dn > Ds and Dn/Ds > 1. We thus examined patterns of nucleotide substitutions within each of the three domains (signal peptide, acidic propiece, and antimicrobial progenitor sequence) of transcripts encoding orthologous Gly-Leu-rich peptides in *P. bicolor*, *P. dacnicolor*, *A. annae*, and *A. callidryas*. The patterns of synonymous substitutions are not the same in the three domains. Dn/Ds increased from the signal peptide (0.09 on average) to propiece (0.296 on average) to antimicrobial progenitor sequence (1.05 on average), and Dn/Ds was greater than 1 within the antimicrobial progenitor sequence. These findings suggest that diversifying (positive) selection has operated within the antimicrobial domain of the Gly-Leu-rich peptide loci in hylids. This agree with previous studies (*83*) showing that positive selection has operated within several other antimicrobial loci in hylids and ranins, as it does among other immunodefense related genes (*84*, *85*). *P. bicolor* and *P. dacnicolor* have different patterns of distribution with respect to geography, climate, and vegetation (*86*). Accordingly, the gain of antimicrobial activity during the evolution of DRP-PBN2 may have been driven, at least in part, by environmental pressure to accelerate the adaptation of *P. bicolor* to the particular noxious microbial fauna that this species encounters. In this context, the presence of numerous antimicrobial peptides in *P. bicolor* skin (the dermaseptins B, phylloxin, dermatoxin, DRP-PBN1, and DRP-PBN2) having distinct but overlapping spectra of antimicrobial activity and acting in synergy could be part of a strategy for providing frogs with the maximum protection against a wide range of infectious microorganisms. Hence, these antimicrobial peptides with such diverse structures and actions can be viewed as the successful evolution of a multidrug defense system, which minimizes the chance of microorganisms developing resistance to individual peptides.

However, the validity of this scenario depends on the assumption that the sequence and activity spectrum of the common ancestor (node A in Figure 2) of DRP-PBN2 and ANC resembled that of ANC. Should this prove not to be correct, ANC and then DRP-PD 3−6 would be a rare example of a loss of function of orthologous proteins. In this context, Dn/Ds ratios equal to or slightly greater than 1 are consistent with the possibility that some of the peptides of the Gly-Leu-rich peptide loci are under neutral evolution; i.e., all of these sequences are liberated from their original functional constraints. Because all of the nonsynonymous and synonymous mutations are then neutral, Dn/Ds will be close or equal to unity and these genes will accept nonsynonymous mutations at a high rate. Accordingly, DRP-PD 3−6 may be part of a bank of variants assembled by random fixation of nonsynonymous mutations, which are available for further diversifying selection when the microbial environment or the genetic background changes.

CONCLUSION

The biosensor, CD spectroscopy, and biological assay results all indicate that evolution has positively selected charge-altering nucleotide substitutions at two sites to generate, among neutral hemolytic peptides, an orthologous cationic variant that binds and permeates bacterial cell membranes. This adds further support to the view that a positive net charge is the major determinant of potent antimicrobial activity in α-helical amphipathic peptides. Several glycines (α-helix breakers with great backbone flexibility) and β-branched amino acids (β-sheet formers) can be accommodated in an amphipathic helix when the helix is in a membrane environment. This is in accordance with the observation that these amino acids are preponderant within transmembrane segments of membrane proteins (*74*). This finding supports the notion that the helical propensity of a given amino acid in a peptide is specified by the context (molecular environment and local amino acid sequence). Furthemore, it is possible that Gly-induced flexibility in the

Gly-Leu-rich peptides facilitates a complete insertion of the entire peptides into the lipid bilayer. The coil−helix transition and helical contents of membrane-bound Gly-Leu-rich peptides is driven by the hydrophobic effect and hydrophobic interactions by reducing the entropy in the peptide and low-dielectric-favoring intrachain hydrogen-bond formation. Hydrophobic interactions between the nonpolar surface of the helix and the acyl chains of the lipids are major contributors to the free energy of binding to both anionic and zwitterionic membranes. In sharp contrast to most known helical and cationic antimicrobial peptides, the high affinity of Gly-Leu-rich peptides for anionic rather than zwitterionic membranes is due to short-range electrostatic interactions that prolong the residence time of the membrane-inserted peptide. This suggests that the interactions of cationic Gly-Leu-rich peptides with bacterial and erythrocyte membranes are dissimilar.

The precise mechanism by which cationic Gly-Leu-rich peptides permeate and disrupt bacterial membranes is still unknown, and clear support for either mechanism of action "channel", "micellar", or "carpet" is beyond the scope of this study. Strikingly, ϑ, the angle subtended by the positively charged residues inDRP-PBN2, is 30°, which is 4−6 time smaller than ϑ of dermaseptins or magainins. It has been shown previously that the smaller the value of ϑ, the higher the capacity of the peptide to insert and disturb the organization of the outer leaflet of anionic membranes (*40*). Therefore, the small angle ϑ combined with high hydrophobicity and flexibility of Gly-Leu-rich cationic peptides might be responsible for their high propensity to bind and, once bound, to reside into the membrane, thereby triggering local fusion of the membrane leaflets, pore-formation cracks, and membrane disruption.

ACKNOWLEDGMENT

The authors thank the Service de Modélisation et Imagerie Moléculaires of the Réseau Fédératif de Recherche of University Paris VI for calculation facilities.

REFERENCES

1. Bai, J. Z., Saafi, E. L., Zhang, S., and Cooper, G. J. (1999) Role of Ca2+ in apoptosis evoked by human amylin in pancreatic islet-cells, *Biochem. J. 343*, 53−61.
2. Mirzabekov, T., Lin, M. C., and Kagan, B. L. (1996) Pore formation by the cytotoxic islet amyloid peptide amylin, *J. Biol. Chem. 271*, 1988−92.
3. Lin, M. C., Mirzabekov, T., and Kagan, B. L. (1997) Channel formation by a neurotoxic prion protein fragment, *J. Biol. Chem. 272*, 44−47.
4. Kagan, B. L., Hirakura, Y., Azimov, R., Azimova, R., and Lin, M. C. (2002) The channel hypothesis of Alzheimer's disease: Current status, *Peptides 23*, 1311−1315.
5. Gallo, R. L., Murakami, M., Ohtake, T., and Zaiou, M. (2002) Biology and clinical relevance of naturally occurring antimicrobial peptides, *J. Allergy Clin. Immunol. 110*, 823−831.
6. Hancock, R. E., and Patrzykat, A. (2002) Clinical development of cationic antimicrobial peptides: from natural to novel antibiotics, *Curr. Drug Targets Infect. Disord. 2*, 79−83.
7. Zasloff, M. (2002) Antimicrobial peptides in health and disease, *New Engl. J. Med. 347*, 1151−60.
8. Kourie, J. I., and Shorthouse, A. A. (2000) Properties of cytotoxic peptide-formed ion channels, *Am. J. Physiol. Cell Physiol. 278*, C1063−1087.
9. Brogden, K. A., Ackermann, M., McCray, P. B., Jr., and Tack, B. F. (2003) Antimicrobial peptides in animals and their role in host defences, *Int. J. Antimicrob. Agents. 22*, 465−78.
10. Kuhn-Nentwig, L. (2003) Antimicrobial and cytolytic peptides of venomous arthropods, *Cell. Mol. Life Sci. 60*, 2651−68.
11. Zasloff, M. (2002) Antimicrobial peptides of multicellular organisms, *Nature 415*, 389−95.
12. Ganz, T. (2001) Antimicrobial proteins and peptides in host defense, *Semin. Respir. Infect. 16*, 4−10.
13. Hancock, R. E. (2001) Cationic peptides: effectors in innate immunity and novel antimicrobial, *Lancet Infect. Dis. 1*, 156−64.
14. Gennaro, R., and Zanett, i M. (2000) Structural features and biological activities of the cathelicidin-derived antimicrobial peptides, *Biopolymers 55*, 31−49.
15. Tossi, A., Sandri, L., and Giangaspero, A. (2000) Amphipathic, alpha-helical antimicrobial peptides, *Biopolymers 55*, 4−30.
16. Bulet, P., Hetru, C., Dimarcq, J. L., and Hoffmann, D. (1999) Antimicrobial peptides in insects; structure and function, *Dev Comp Immunol. 23*, 329−44.
17. Epand, R. M., and Vogel, H. J. (1999) Diversity of antimicrobial peptides and their mechanisms of action, *Biochim. Biophys. Acta 1462*, 11−28.
18. Andreu, D., and Rivas, L. (1998) Animal antimicrobial peptides: an overview, *Biopolymers 47*, 415−33.
19. Simmaco, M., Mignogna, G., and Barra, D. (1998) Antimicrobial peptides from amphibian skin: what do they tell us?, *Biopolymers 47*, 435−50.
20. Brahmachary, M., Krishnan, S. P., Koh, J. L., Khan, A. M., Seah, S. H., Tan, T. W., Brusic, V., and Bajic, V. B. (2004) ANTIMIC: a database of antimicrobial sequences, *Nucleic Acids Res. 32*, D586−9.
21. Wang, Z., and Wang, G. (2004) APD: the antimicrobial peptide database, *Nucleic Acids Res. 32*, D590−2.
22. Wade, D., and Englund, J. (2002) Synthetic antibiotic peptides database, *Protein Pept. Lett. 9*, 53−7.
23. Tossi, A. A database with more than 400 entries. http///www.bbcm. univ. trieste.it/∼tossi/search.html.
24. Ehrenstein, G., and Lecar, H. (1977) Electrically gated ionic channels in lipid bilayers, *Q. Rev. Biophys. 10*, 1−34.
25. Pouny, Y., Rapaport, D., Mor, A., Nicolas, P., and Shai, Y. (1992) Interaction of antimicrobial dermaseptin and its fluorescently labeled analogues with phospholipids membranes, *Biochemistry 31*, 12416−23.
26. Matsuzaki, K. (1998) Magainins as paradigm for the mode of action of pore forming polypeptides, *Biochim. Biophys. Acta 1376*, 391−400.
27. Hancock, R. E. (1999) Peptide antibiotics, *Antimicrob. Agents Chemother. 93*, 1317−23.
28. Huang, H. W. (2000) Action of antimicrobial peptides: 2-state model, *Biochemistry 39*, 8347−52.
29. Shai, Y. (2002) Mode of action of membrane active antimicrobial peptides, *Biopolymers 66*, 236−48.
30. Conlon, J. M., Kolodziejek, J., and Nowotny, N. (2004) Antimicrobial peptides from ranid frogs: taxonomic and phylogenetic markers and a potential source of new therapeutic agents, *Biochim. Biophys. Acta 1696*, 1−14.
31. Apponyi, M. A., Pukala, T. L., Brinkworth, C. S., Maselli, V. M., Bowie, J. H., Tyler, M. J., Booker, G. W., Wallace, J. C., Carver, J. A., Separovic, F., Doyle, J., and Llewellyn, L. E. (2004) Host-defense peptides of Australian Anurans: structure, mechanism of action and evolutionary significance, *Peptides*, in press.
32. Nascimento, A. C., Fontes, W., Sebben, A., and Castro, M. S. (2003) Antimicrobial peptides from anurans skin secretions, *Protein Pept. Lett. 10*, 227−38.
33. Nicolas, P., Vanhoye, D., and Amiche, M. (2003) Molecular strategies in biological evolution of antimicrobial peptides, *Peptides 24*, 1669−80.
34. Rinaldi, A. C. (2002) Antimicrobial peptides from amphibian skin: an expanding scnenario, *Curr. Opin. Chem. Biol. 6*, 799−804.
35. Nicolas, P., and Mor, A. (1995) Peptides as weapons against microorganisms in the chemical defense system of vertebrates, *Annu. Rev. Microbiol. 49*, 277−304.
36. Park, I. Y., Cho, J. H., Kim, K. S., Kim, Y. B., and Kim, S. C. (2004) Helix stability confers salt resistance upon helical antimicrobial peptides, *J. Biol. Chem.*
37. Dennison, S. R., Harris, F., and Phoenix, D. A. (2003) Factors determining the efficacy of alpha helical antimicrobial peptides, *Protein Pept. Lett. 10*, 497−502.

38. Papo, N., and Shai, Y. (2003) Can we predict biological activity of antimicrobial peptides from their interactions with model phospholipid membranes? *Peptides 24*, 1693−703.
39. Powers, J. P., and Hancock, R. E. (2003) The relationship between peptide structure and antibacterial activity, *Peptides 24*, 1681−91.
40. Dathe, M. Meyer, J., Beyermann, M., Maul, B., Hoischen, C., and Bienert, M. (2002) General aspects of peptide selectivity towards lipid bilayers and cell membranes studied by variation of the structure parameters of amphipathic helical model peptides, *Biochim. Biophys. Acta 1558*, 171−86.
41. Kustanovich, I., Shalev, D. E., Mikhlin, M., Gaidukov, L., and Mor, A. (2002) Structural requirements for potent versus selective cytotoxicyty for antimicrobial dermaseptin S4 derivatives, *J. Biol. Chem. 277*, 16941−51.
42. Tochi, T., Epand, R. F., Epand, R. M., and Matsuzaki, K. (2002) Position-dependent hydrophobicity of the antimicrobial magainin peptide affects the mode of peptide-lipid interaction and selectivity, *Biochemistry 41*, 10723−31.
43. Giangaspero, A., Sandri, L., and Tossi, A. (2001) Amphipathic alpha helical peptides, *Eur. J. Biochem. 268*, 5589−600.
44. Bechinger, B. (1999) The structure, dynamics and orientation of antimicrobial peptides in membranes by multidimensional solid-phase NMR spectroscopy, *Biochim. Biophys. Acta 1462*, 157−83.
45. Blondelle, S. E., Lohner, K., and Aguilar, M. (1999) lipid-induced conformation and lipid binding properties of cytolytic and antimicrobial peptides: determination and biological specificity, *Biochim. Biophys. Acta 1462*, 89−108.
46. Matsuzaki, K. (1999) Why and how are peptide-lipid interactions utilized for self-defense? Magainins and tachyplesins as archetypes, *Biochim. Biophys. Acta 1462*, 1−10.
47. Sitaram, N., and Nagaraj, R. (1999) Interaction of antimicrobial peptides with biological and model membranes: structural and charge requirements for activity, *Biochim. Biophys. Acta 1462*, 29−54.
48. Shai, Y. (1999) Mechanism of the binding, insertion and destabilization of phospholipid bilayer membranes by alpha-helical antimicrobial and cell nonselective membrane-lytic peptides, *Biochim. Biophys. Acta 1462*, 55−70.
49. Hwang, P. M., and Vogel, H. J. (1998) Structure−function relationships of antimicrobial peptides, *Biochem. Cell. Biol. 76*, 235−46.
50. Lai, R., Liu, H., Hui Lee, W., Zhang, Y. (2002) An anionic antimicrobial peptide from toad *Bombina maxima*, *Biochem. Biophys. Res. Commun. 295*, 796−9.
51. Zhang, J., and Rosenberg, H. (2002) Complementary advantageous substitutions in the evolution of an antiviral Rnase of higher primates, *Proc. Natl. Acad. Sci. U.S.A. 99*, 5486−91.
52. Amiche, M., Séon, A., Pierre, T. N., Nicolas, P. (1999) The dermaseptin precursors: a protein family with a common preproregion and a variable C-terminal antimicrobial domain, *FEBS Lett. 456*, 352−6.
53. Chen, T., Tang., L., and Shaw, C. (2003) Identification of three novel *Phyllomedusa sauvagei* dermaseptins by cloning from a skin secretion-derived cDNA library, *Regul. Peptides 116*, 139−46.
54. Brand, G. D., Leite, J. R., Silva, L. P., Albuquerque, S., Prates, M. V., Azevedo, R. B., Carregaro, V., Da Silva, J. S., Sa, V. C., Brandao, R. A., and Bloch, C. Jr. (2002) Dermaseptins from *Phyllomedusa oreades* and *Phyllomedusa distincta*. Anti-*Trypanosoma cruzi* activity without cytotoxicity to mammalian cells, *J. Biol. Chem. 277*, 49332−40.
55. Wechselberger, C. (1998) Cloning of cDNAs encoding new peptides of the dermaseptin-family, *Biochim. Biophys. Acta 1388*, 279−83.
56. Charpentier, S., Amiche, M., Mester, Y., Vouille, V., Le Caer, J. P., Nicolas, P., and Delfour, A. (1998) Structure, Synthesis and molecular cloning of dermaseptins B, a family of skin peptide antibiotics, *J. Biol. Chem. 273*, 14690−96.
57. Sambrook, J., Fritsch, E. F., and Maniatis, T. (1989) Molecular cloning. A Laboratory manual, 2nd ed. Cold Spring Harbor laboratory, Cold Spring Harbor, NY.
58. Thompson, J. D., Gibson, T. J., Plewniak, F., Jeanmougin, F., and Higgins, D. G. (1997) The CLUSTAL X windows interface: flexible strategies for multiple sequence alignment aided by quality analysis tools, *Nucleic Acids Res. 24*, 4876−82.
59. Kimura, M. (1980) A simple method for estimating evolutionary rates of base substitutions through comparative studies of nucleotide sequences, *J. Mol. Evol. 16*, 111−20.
60. Swofford, D. L. (1999) PAUP: phylogenetic analysis using parsimony and other methods. Version 4. Sinauer Associates. Sunderland, Mass
61. Ina, Y. (1995) New methods for estimating the numbers of synonymous and nonsynonymous substitutions, *J. Mol. Evol. 40*, 190−226.
62. Jukes, T. H., and Cantor, C. R. (1969) Evolution of protein molecules, pp 21−132 in Mammalian Protein Metabolism, ed. H. N. Munro. Academic Press, New York.
63. Pierre, T. N., Seon, A. A., Amiche, M., and Nicolas, P. (2000) Phylloxin, a novel peptide antibiotic of the dermaseptin family of antimicrobial/opioid peptide precursors, *Eur. J. Biochem. 267*, 370−8.
64. Wilm, M., and Mann, M. (1996) Analytical properties of the nanoelectrospray ion source, *Anal. Chem. 68*, 1−8
65. Roepstorff, P., and Fohlman, M. (1984) Proposal for a common nomenclature for sequence ions in mass spectra of peptides, *J. Biomed. Mass. Spectrom. 11*, 601−6.
66. Honig, B., and Nicholls, A. (1995) Classical electrostatics in biology and chemistry, *Science 268*, 1144−49.
67. Hagler, A. T., Stren, P. S., Sharon, R., Becker, J. M., and Naider, F. (1979) Computer simulation of the conformational properties of oligopeptides. Comparison of the theoretical methods and analysis of experimental results, *J. Am. Chem. Soc 101*, 6842−52.
68. Amiche, M., Séon, A., Wroblewski, H., and Nicolas, P. (2000) Isolation of dermatoxin from frog skin, an antibacterial peptide encoded by a novel member of the dermaseptin genes family, *Eur. J. Biochem. 267*, 4583−92.
69. Matsuzaki, K., Murase, O., Sugishita, K., Yoneyama, S., Akada, K., Ueha, M., Nakamura, A., and Kobayashi, S. (2000) Optical characterization of liposomes by right angle light scattering and turbidity measurements. *Biochim. Biophys. Acta Biomembranes 1467*, 219−226.
70. Zhong, L., and Johnson, W. C., Jr. (1992) Environment affects amino acid preference for secondary structure, *Proc. Natl. Acad. Sci. U S A. 89*, 4462−65.
71. Mozsolits H., Wirth H. J., Werkmeister J, and Aguilar M. I. (2001) Analysis of antimicrobial peptide interactions with hybrid bilayer membrane systems using surface plasmon resonance, *Biochim. Biophys. Acta 1512*, 64−76.
72. Deleage, G., Blanchet, C., and Geourjon, C. (1997) Secondary consensus prediction. Protein structure prediction. Implications for the biologist, *Biochimie 79*, 681−6.
73. Li, S. C., Kim, P. K., and Deber, C. M. (1995) Manipulation of peptide conformations by fine-tuning of the environment and/or the primary sequence, *Biopolymers 35*, 667−75.
74. Li, S. C., and Deber, C. M. (1992) Glycine and β-branched residues support and modulate peptide helicity in membrane environments, *FEBS Lett. 311*, 217−20.
75. Johnson, J. E., Xie, M., Singh, L. M. R., Edge, R., and Cornell, R. (2003) Both acidic and basic amino acids in an amphitropic enzyme CTP: phosphocholine cytidyltransferase, dictate its selectivity for anionic membranes, *J. Biol. Chem. 278*, 514−22.
76. Segrest, J. P., De Loof, H., Dohlman, J. G., Brouillette, C. G., and Anantharamaiah, G. M. (1990) Amphipathic helix motif: classes and properties, *Proteins 8*, 103−17.
77. Gaidukov, L., Fish, A., and Mor, A. (2003) Analysis of membrane-binding properties of dermaseptin analogues: relationships between binding and cytotoxicity, *Biochemistry 42*, 12866−74.
78. Chia, C. S. B., Torres, J., Cooper, M. A., Arkin, I. T., and Bowie, J. H. (2002) The orientation of the antibiotic peptide maculatin 1.1 in DMPG and DMPC lipid bilayers. Support for a pore-forming mechanism, *FEBS Lett. 512*, 47−51.
79. Papo, N., and Shai, Y. (2003) Exploring peptide membrane interaction using surface plasmon resonance: differentiation between pore formation versus membrane disruption by lytic peptides, *Biochemistry 42*, 458−66.
80. Blondelle, S. E., Lohner, K., and Aguilar, M. (1999) Lipid-induced conformation and lipid-binding properties of cytolytic and antimicrobial peptides: determination and biological specificity, *Biochim. Biophys. Acta 1462*, 89−108.
81. Hicks, R. P., Mones, E., Kim, H., Koser, B. W., Nichols, D. A., and Bhattacharjee, A. K. (2003) Comparison of the conformation and electrostatic surface properties of magainin peptides bound

to sodium dodecyl sulfate and dodecylphosphocholine micelles, *Biopolymers 68*, 459−70.
82. Lequin, O., Bruston, F., Convert, O., Chassaing, G., and Nicolas, P. (2003) Helical structure of dermaseptin B2 in a membrane-mimetic environment, *Biochemistry 42*, 10311−10323.
83. Duda, T. F., Vanhoye, D., and Nicolas, P. (2002) Roles of diversifying selection and coordinated evolution in the evolution of amphibian antimicrobial peptides, *Mol. Biol. Evol. 19*, 858−864.
84. Ota, T., Sitnikova, T., and Nei, M. (2000) Evolution of vertebrate immunoglobulin variable gene segments, *Curr. Top. Microbiol. Immunol. 248*, 221−245.
85. Hughes, A. L. (1997) Rapid evolution of immunoglobulin superfamily C2 domains expressed in immune system cells, *Mol. Biol. Evol. 14*, 1−5.
86. Duellman, W. E., and Trueb, L. (1994) *Biology of Amphibians*, John Hopkins University Press, London, U.K.
87. Simmaco, M., Mignogna, G., Barra, D., and Bossa, F. (1994) Antimicrobial peptides from skin secretions of *Rana esculenta*. Molecular cloning of cDNAs encoding esculentin and brevinins and isolation of new active peptides, *J. Biol. Chem. 269*, 11956−11961.

BI0493158